Electronic Supplementary Information

Pillar[5]arenes decorated with six-membered-ring aromatics at all the substitution positions

Tomoya Kaneda,[a] Kenichi Kato,*[a] Shunsuke Ohtani [a] and Tomoki Ogoshi*[a,b]

[a] Department of Synthetic Chemistry and Biological Chemistry, Graduate School of Engineering, Kyoto University, Nishikyo-ku, Kyoto, 615-8510, Japan

E-mail: katok@sbchem.kyoto-u.ac.jp, ogoshi@sbchem.kyoto-u.ac.jp

[b] WPI Nano Life Science Institute, Kanazawa University, Kakuma-machi, Kanazawa, 920-1192, Japan

Contents

1. General information
2. Synthetic procedures and compound data
3. ^{1}H and ^{13}C NMR spectra
4. High-resolution APCI-FT-MS
5. X-Ray crystallographic analysis
6. UV/vis absorption and fluorescence spectra
7. HPLC charts and chiroptical measurement
8. Theoretical calculations
9. References
10. Additional information

1. General information

Material in Synthesis

All reagents and solvents were of commercial reagent grade and were used without further purification except where noted. Dehydrated *N*,*N*-dimethylformamide (DMF, Super) was purchased from Kanto Chemical Co., Inc. Super dehydrated 1,4-dioxane and palladium(II) acetate [$Pd(OAc)_2$] were purchased from FUJIFILM Wako Pure Chemical Industry, Ltd. Pd-PEPSSI-iPr was purchased from Tokyo Chemical Industry Co., Ltd. XPhos Pd G3 was purchased from Sigma-Aldrich Co. LLC. Deionized water was obtained from a Merck Elix-Essential-3 instrument with a Progard TS2 Pretreatment Pack. Preparative silica gel and chromatography was performed on Wakosil 60. Gel Permeation Chromatography (GPC) was performed on a Japan Analytical Industry LaboACE LC-5060 recycling HPLC apparatus equipped with two JAIGEL-2HR columns, using $CHCl_3$ (containing EtOH) as eluent.

Instrumental

^{1}H (600 MHz, 500 MHz, 400 MHz), ^{13}C (151 MHz, 126 MHz, 100 MHz), and ^{19}F (471 MHz) NMR spectra were recorded on JEOL ECZ600R, ECZ500R, and ECS400 spectrometers. Chemical shifts were reported as the delta scale in ppm relative to the internal standards (δ = 7.26 ppm for ^{1}H and 77.16 ppm for ^{13}C in $CDCl_3$ and δ = 5.32 ppm for ^{1}H in CD_2Cl_2) or external standard (sodium trifluoromethanesulfonate (CF_3SO_3Na), δ = −78.8 ppm for ^{19}F).

High-resolution atmospheric pressure chemical ionization Fourier transform (HR APCI-FT) mass spectra were recorded on a Thermo Fisher Scientific LTQ orbitrap XL instrument using the APCI method in positive ion mode. High-resolution electrospray ionization Fourier transform (HR ESI-FT) mass spectra were recorded on a Thermo Fisher Scientific EXACTIVE Plus instrument using the ESI method in positive ion mode.

Single-crystal X-ray diffraction analyses were performed on a Rigaku MicroMax-007HF apparatus at −130 °C using two-dimensional detector Saturn 724HG with Mo-Kα radiation (λ = 0.71073 Å). The structures were solved by direct method SHELXS-2013/1 and refined by SHELXL-2018/3 program.[S1,S2]

Ultraviolet/visible (UV/vis) absorption spectra were recorded on a JASCO V-750 spectrophotometer. Optical separations were performed on a Japan Analytical Industry LaboACE LC-5060 recycling HPLC apparatus equipped with two DAICEL CHIRALPAK IA (ϕ = 10 mm, l = 250 mm) columns and the obtained fractions as well as racemic samples were analyzed on a Hitachi Chromaster HPLC instrument equipped with a DAICEL CHIRALPAK IA (ϕ = 4.6 mm, l = 250 mm) column. Circular dichroism (CD) spectra were recorded on a JASCO J-1500 circular dichroism spectrometer. Fluorescence spectra were measured on a JASCO FP-8550 spectrofluorometer. Absolute fluorescence quantum yields were determined on a Hamamatsu Photonics Quantaurus-QY C11347 absolute PL quantum yield spectrometer.

Theoretical calculations were carried out using the *Gaussian 16* program.[S3] The single-crystal structure of **P5Ph** was fully optimized without any restriction by the density functional theory (DFT) method with RB3LYP level,[S4] employing a basis set 6-31G(d). After the optimization, electronic states and transitions were computed with TD-SCF/RωB97X-D level,[S5] employing a basis set 6-31G(d,p). After replacement of *para* hydrogen atoms of the single-crystal structure of **P5Ph** with methyl groups or fluorine atoms, the same optimization and TD-SCF energy calculations were performed.

2. Synthetic procedures and compound data

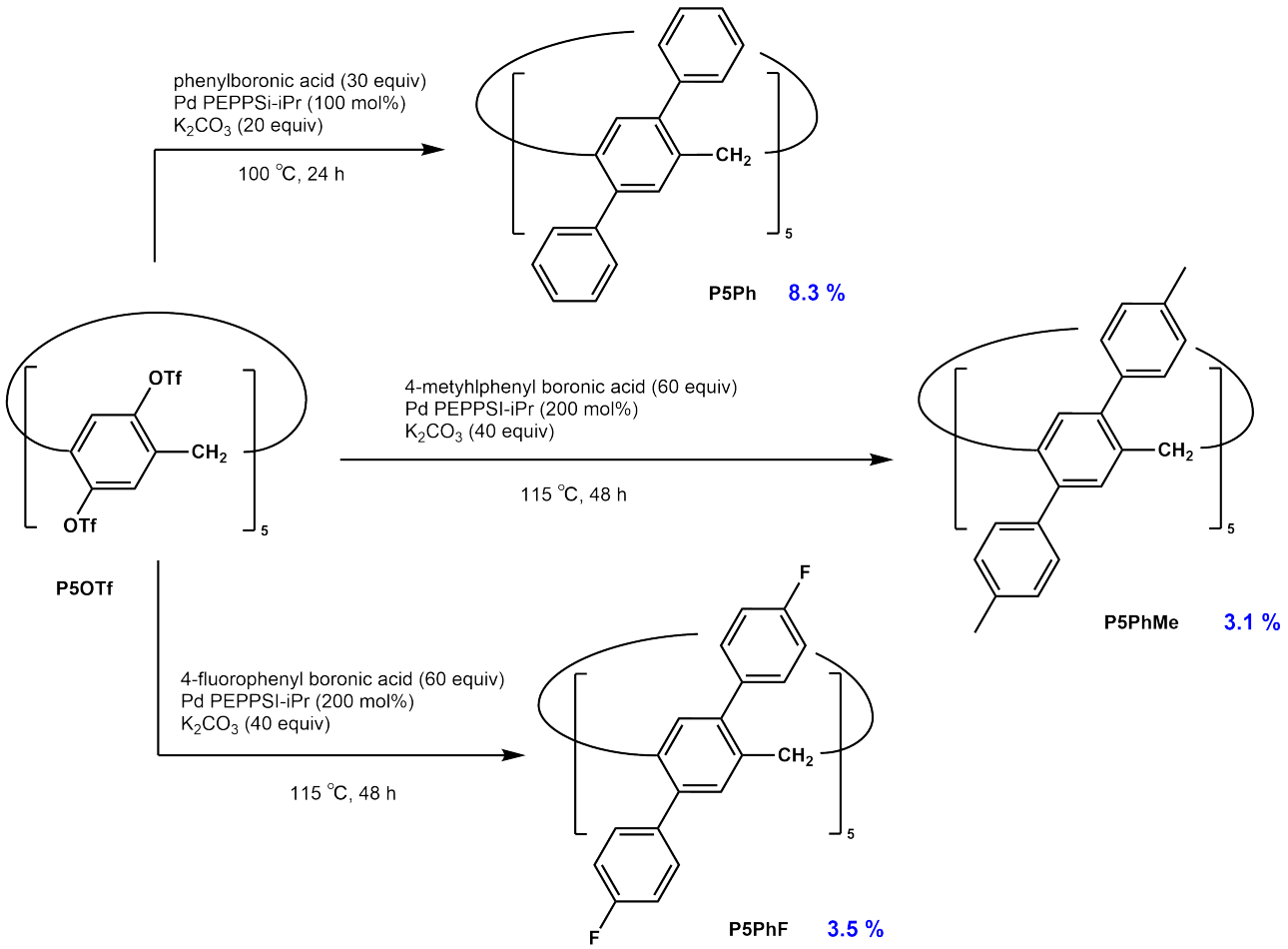

Scheme S2-1. Synthesis of per-aryl-substituted pillar[5]arenes. **P5OTf** was synthesized following a reported procedure.[S6]

General procedure for Suzuki–Miyaura coupling

Per-triflate-substituted pillar[5]arene (**P5OTf**), Pd-PEPPSI-iPr, boronic acid, and K_2CO_3 were placed in a 50 mL two-neck round-bottom flask, to which solvents were added under a nitrogen atmosphere. After heating with stirring, the mixture was quenched with H_2O. The mixture was extracted with dichloromethane three times. The organic extracts were dried over anhydrous Na_2SO_4, and the solvent was evaporated under reduce pressure.

Per-phenyl-substituted pillar[5]arene (P5Ph): **P5Ph** was prepared according to the General procedure for Suzuki–Miyaura coupling, using **P5OTf** (20 mg, 0.010 mmol), phenylboronic acid (36 mg, 0.30 mmol), Pd-PEPPSI-iPr (7.0 mg, 0.010 mmol), K_2CO_3 (30 mg, 0.20 mmol), and 1,4-dioxane (2.0 mL). The crude product was separated using column chromatography on silica gel (CH_2Cl_2/*n*-hexane = 2/1) and recrystallization from CH_2Cl_2/*n*-hexane, affording **P5Ph** (1.0 mg, 0.00083 mmol, 8.3%) as white solids. ^{1}H NMR (600 MHz,

$CDCl_3$, 298 K): δ/ppm = 7.18 (mt, 30H, 3,4-Ph-H), 6.97 (mt, 20H, 2-Ph-H), 6.30 (s, 10H, pillar[5]arene-H), 3.97 (s, 10H, $C\underline{H}_2$); ^{13}C NMR (126 MHz, $CDCl_3$, 298 K): δ/ppm = 141.64, 140.40, 136.33, 132.30, 129.23, 127.98, 126.56, 29.67; HR APCI-FT-MS: *m*/*z* calcd for $[C_{95}H_{71}]^+$: 1211.5550 $[M+H]^+$; found 1211.5544; UV/vis ($CHCl_3$): λ_{max}/nm (ε/M^{-1} cm^{-1}) = 256 (5.6×10^4); FL ($CHCl_3$, Φ_{lum} = 0.18): λ_{max}/nm = 356; 1st fraction (>98%), CD ($CHCl_3$): λ_{max}/nm ($\Delta\varepsilon$/M^{-1} cm^{-1}, g_{abs}) = 263 (111, 2×10^{-3}); 2nd fraction (>98%), CD ($CHCl_3$): λ_{max}/nm ($\Delta\varepsilon$/M^{-1} cm^{-1}, g_{abs}) = 263 (−104, -2×10^{-3}).

Table S2-1. Scope of the per-arylation of pillar[5]arene triflate.

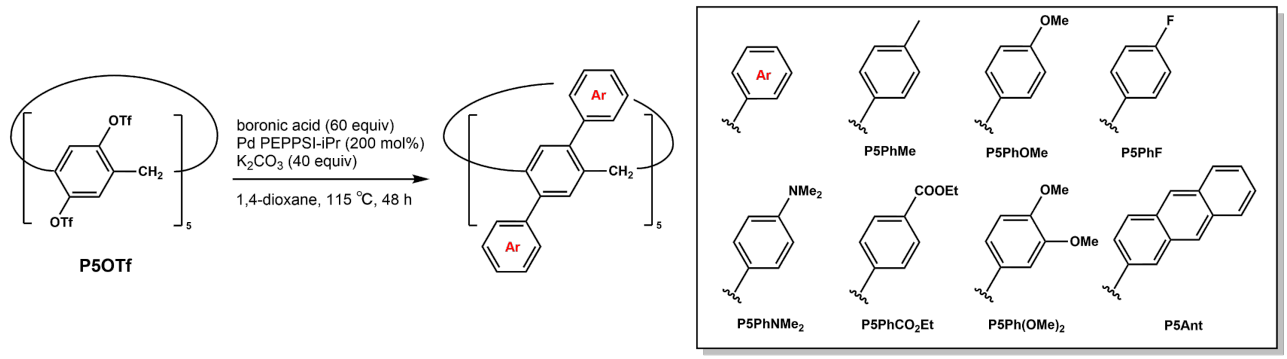

entry	boronic acid	product	yield
1	4-methylphenylboronic acid	**P5PhMe**	3.1%
2	4-methoxyphenylboronic acid	**P5PhOMe**	–[a]
3	4-fluorophenylboronic acid	**P5PhF**	3.5%
4	4-(dimethylamino)phenylboronic acid	**P5PhNMe$_2$**	ND
5	4-(ethoxycarbonyl)phenylboronic acid	**P5PhCO$_2$Et**	ND
6	3,4-dimethoxyphenylboronic acid	**P5Ph(OMe)$_2$**	ND
7	anthracene-2-boronic acid	**P5Ant**	ND

[a] Mass and ^1H NMR spectra confirmed this compound, but the isolation was not successful.

Per-*p*-tolyl-substituted pillar[5]arene (P5PhMe): P5PhMe was prepared according to the General procedure for Suzuki–Miyaura coupling, using **P5OTf** (20 mg, 0.010 mmol), 4-methylphenylboronic acid (82 mg, 0.60 mmol), Pd-PEPPSI-iPr (14 mg, 0.020 mmol), K_2CO_3 (60 mg, 0.40 mmol), and 1,4-dioxane (5.0 mL). The crude product was separated using column chromatography on silica gel (CH_2Cl_2/*n*-hexane = 1/3) and recrystallization from CH_2Cl_2/*n*-hexane, affording **P5PhMe** (0.42 mg, 0.00031 mmol, 3.1%) as white solids. ^1H NMR (400 MHz, $CDCl_3$, 298 K): δ/ppm = 6.96 (d, *J* = 8.0 Hz, 20H, Ar-H), 6.81 (d, *J* = 8.0 Hz, 20H, Ar-H), 6.23 (s, 10H, pillar[5]arene-H), 3.96 (s, 10H, $C\underline{H}_2$), 2.28 (s, 30H, $C\underline{H}_3$); ^{13}C NMR (126 MHz, $CDCl_3$, 298 K): δ/ppm = 140.07, 138.76, 136.05, 135.89, 132.29, 129.15, 128.73, 36.24, 21.14; HR APCI-FT-MS: *m*/*z* calcd for $[C_{105}H_{91}]^+$: 1351.7115 $[M+H]^+$; found 1351.7093; UV/vis ($CHCl_3$): λ_{max}/nm = 257; FL ($CHCl_3$, Φ_{lum} = 0.17): λ_{max}/nm = 357; 1st fraction (>99%), CD ($CHCl_3$): λ_{max}/nm (g_{abs}) = 264 (2×10^{-3}); 2nd fraction (>99%), CD ($CHCl_3$): λ_{max}/nm (g_{abs}) =

263 (-2×10^{-3}).

Per-4-fluorophenyl-substituted pillar[5]arene (P5PhF): P5PhF was prepared according to the General procedure for Suzuki–Miyaura coupling, using **P5OTf** (20 mg, 0.010 mmol), 4-fluorophenylboronic acid (84 mg, 0.60 mmol), Pd-PEPPSI-iPr (14 mg, 0.020 mmol), K_2CO_3 (60 mg, 0.40 mmol), and 1,4-dioxane (5.0 mL). The crude product was separated using column chromatography on silica gel (CH_2Cl_2/*n*-hexane = 1/3) and chiral HPLC (CH_2Cl_2/*n*-hexane = 1/5), affording **P5PhF** (0.50 mg, 0.00036 mmol, 3.5%) as white solids. ^{1}H NMR (500 MHz, $CDCl_3$, 298 K): δ/ppm = 6.89 (mt, 20H, Ar-H), 6.88 (br, 20H, Ar-H), 6.27 (s, 10H, pillar[5]arene-H), 3.90 (s, 10H, C<u>H</u>$_2$); ^{13}C NMR (151 MHz, $CDCl_3$, 298 K): δ/ppm = 161.3 (d, $^1J_{C-F}$ = 246 Hz), 139.7, 137.1 (d, $^4J_{C-F}$ = 3 Hz), 136.5, 132.3, 130.5 (d, $^3J_{C-F}$ = 8 Hz), 115.1 (d, $^2J_{C-F}$ = 21 Hz), 36.0; ^{19}F NMR (471 MHz, $CDCl_3$, 298K): δ/ppm = −115.76 (mt); HR APCI-FT-MS: *m*/*z* calcd for $[C_{95}H_{61}F_{10}]^+$: 1390.4530 $[M+H]^+$; found 1390.4494; UV/vis ($CHCl_3$): λ_{max}/nm = 255; FL ($CHCl_3$, Φ_{lum} = 0.10): λ_{max}/nm = 351; 1st fraction (>99%), CD ($CHCl_3$): λ_{max}/nm (g_{abs}) = 260 (2×10^{-3}); 2nd fraction (>98%), CD ($CHCl_3$): λ_{max}/nm (g_{abs}) = 260 (-2×10^{-3}).

3. ^{1}H and ^{13}C NMR spectra

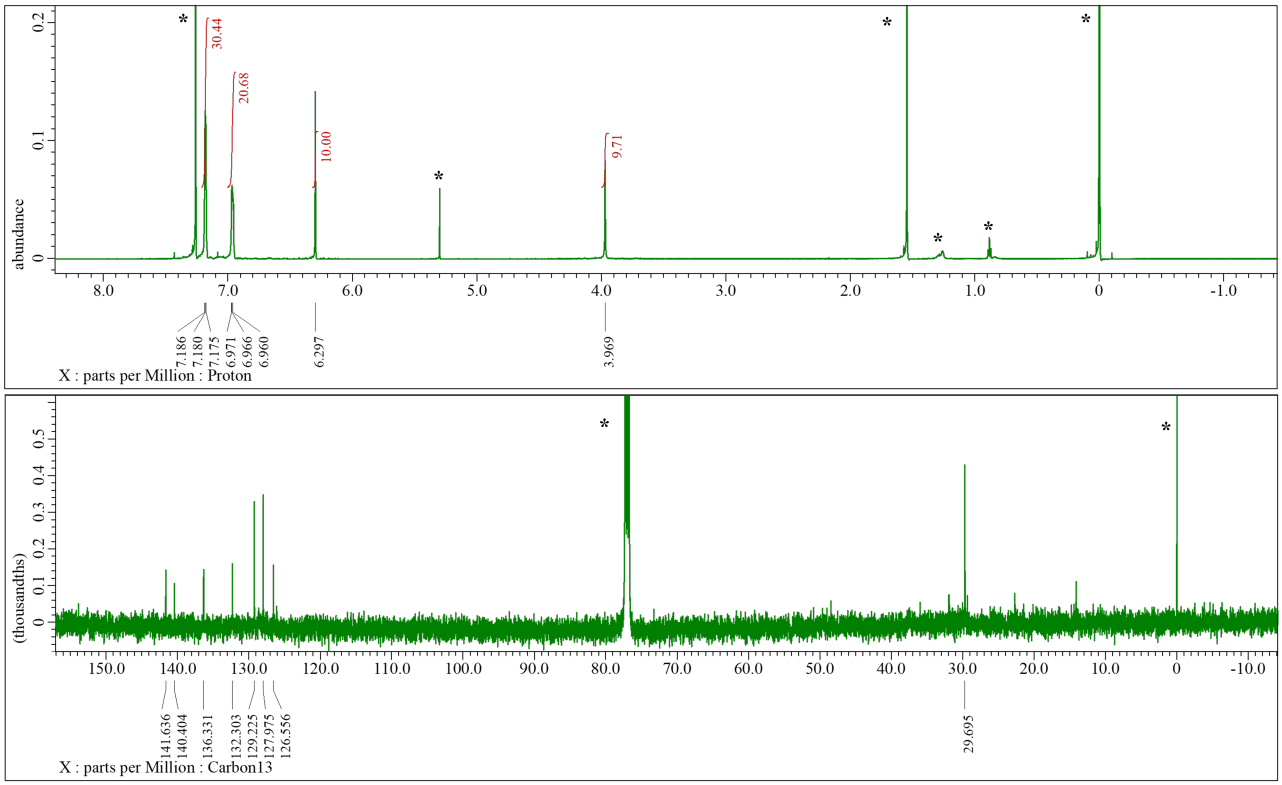

Figure S3-1. ^{1}H (600 MHz) and ^{13}C (126 MHz) NMR spectra of **P5Ph** in $CDCl_3$ at 25 °C. Peaks marked with * are due to residual solvents.

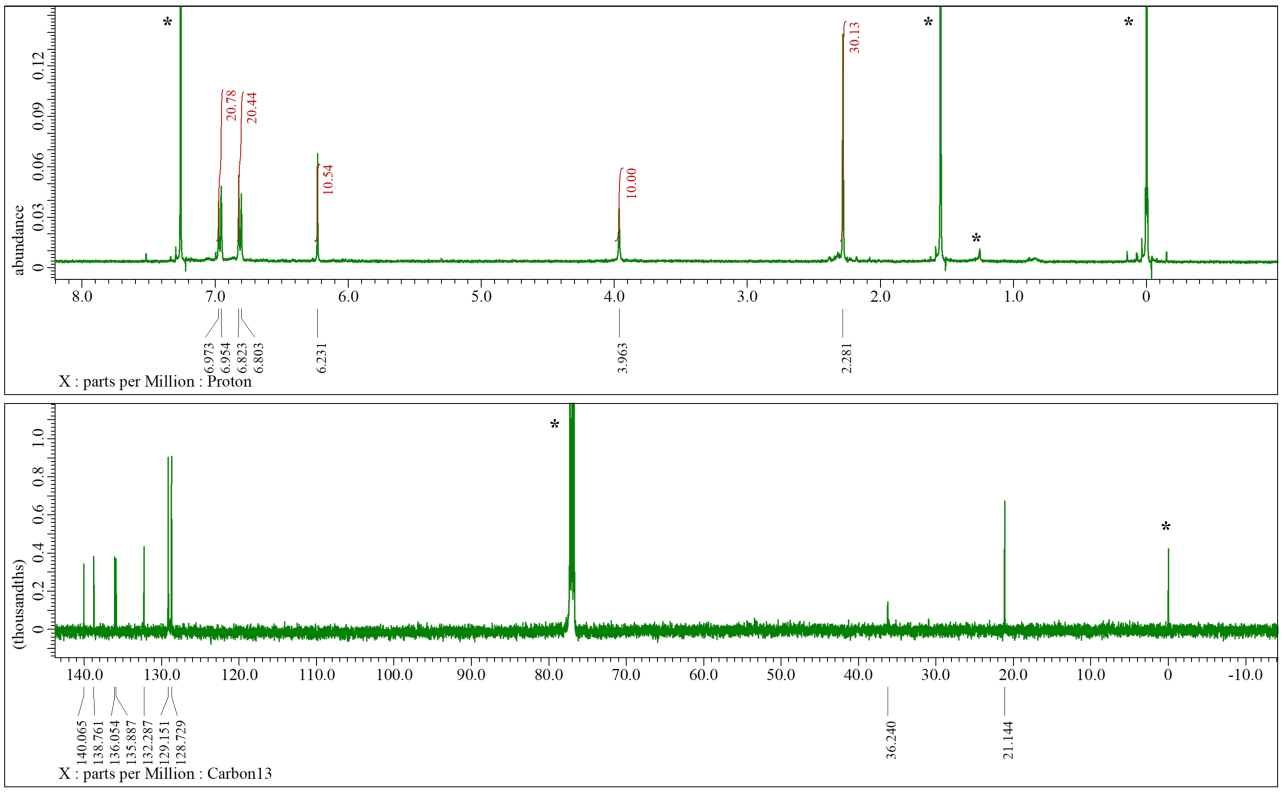

Figure S3-2. ^{1}H (400 MHz) and ^{13}C (126 MHz) NMR spectra of **P5PhMe** in $CDCl_3$ at 25 °C. Peaks marked with * are due to residual solvents.

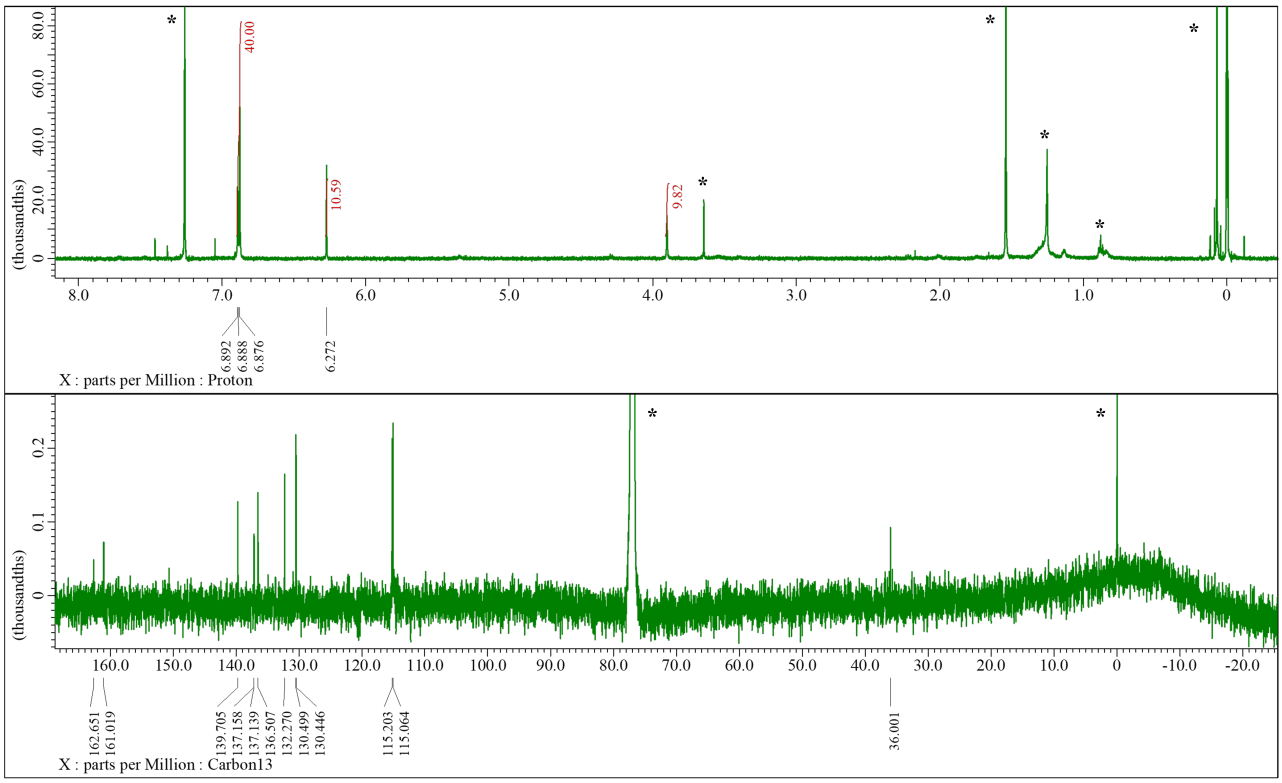

Figure S3-3. ^{1}H (500 MHz) and ^{13}C (151 MHz) NMR spectra of **P5PhF** in $CDCl_3$ at 25 °C. Peaks marked with * are due to residual solvents.

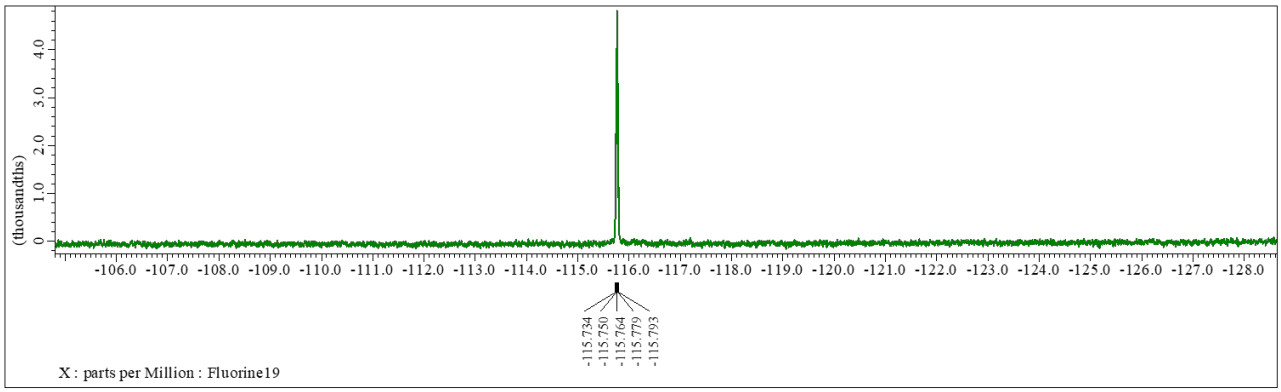

Figure S3-4. ^{19}F (471 MHz) NMR spectrum of **P5PhF** in $CDCl_3$ at 25 °C.

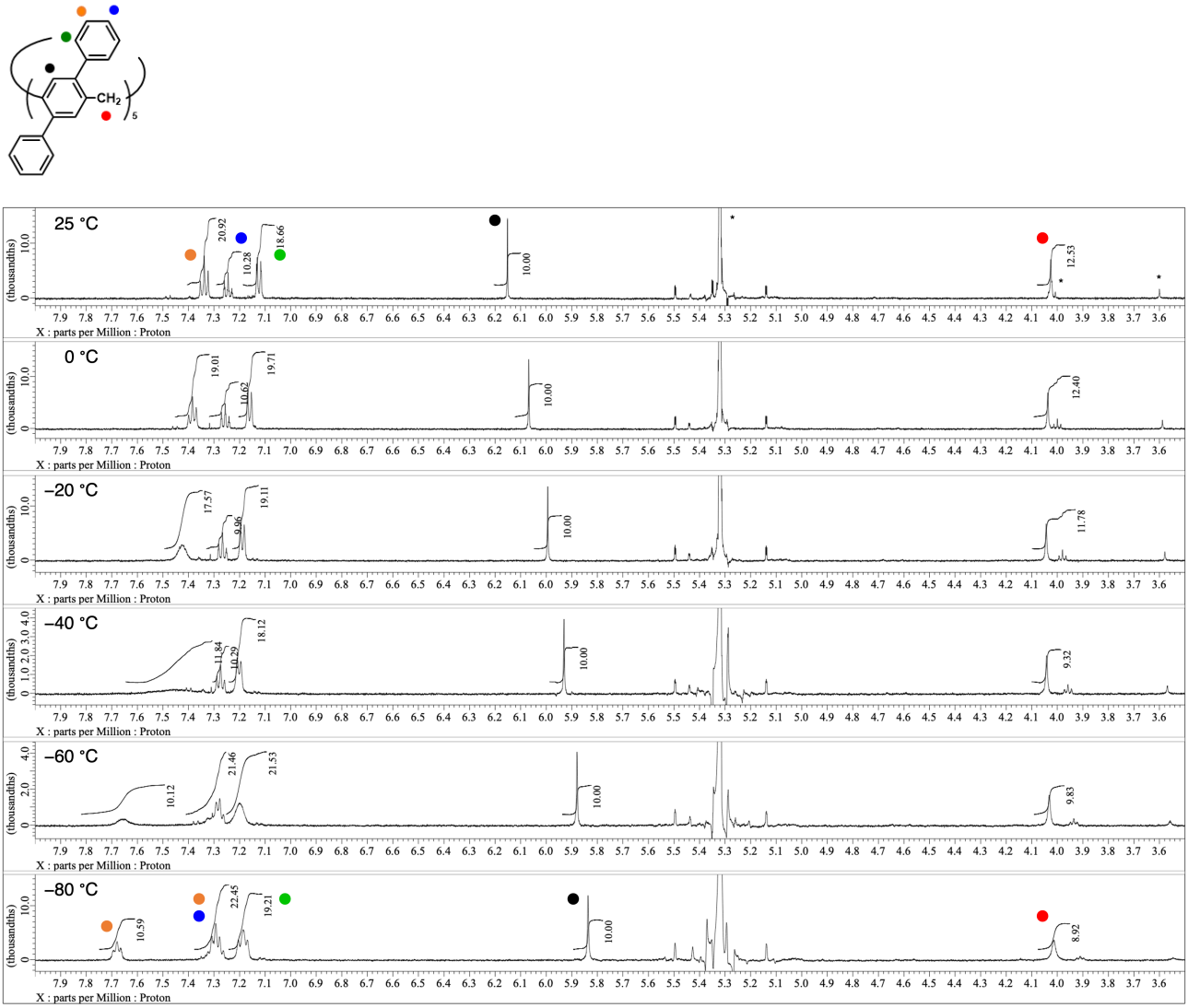

Figure S3-5. Variable-temperature ^{1}H (500 MHz) NMR spectra of **P5Ph** in CD_2Cl_2 at 25 °C to −80 °C. Peaks marked with * are due to residual solvents. Suppressed rotation of the peripheral phenyl substituents caused additional peak splitting of their *ortho*- and *meta*-protons at low temperature. The proton on core benzene ring showed a large change in the chemical shift owing to varied shielding effect by the phenyl substituents but no peak splitting with the retention of D_5-symmetry.

We acquired the ^{1}H NMR using the same sample and scan of 8. The integral values of pillar[5]arene aromatic peaks at around 6 ppm were indeed 0.39–0.42 compared with those for tetramethylsilane. However, "Recvr Gain" values were automatically set at 56 for the spectra at −40 and −60 °C and 66 for the others. Because of this issue, we displayed the spectra at −40 and −60 °C with a different vertical scale giving almost the same heights of tetramethylsilane peaks.

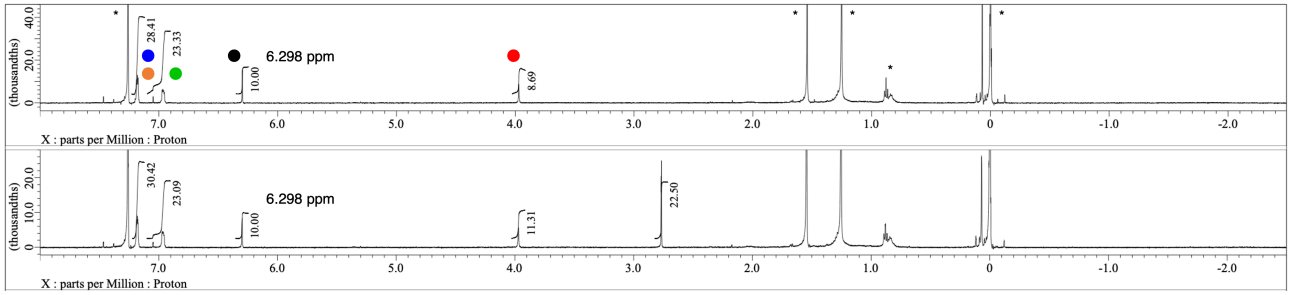

Figure S3-6. Comparison of ^{1}H (500 MHz) NMR spectra of **P5Ph** (0.5 mM) before (top) and after (bottom) addition of 1,2-dicyanoethane (11 equiv) in $CDCl_3$ at 25 °C. Peaks marked with * are due to residual solvents.

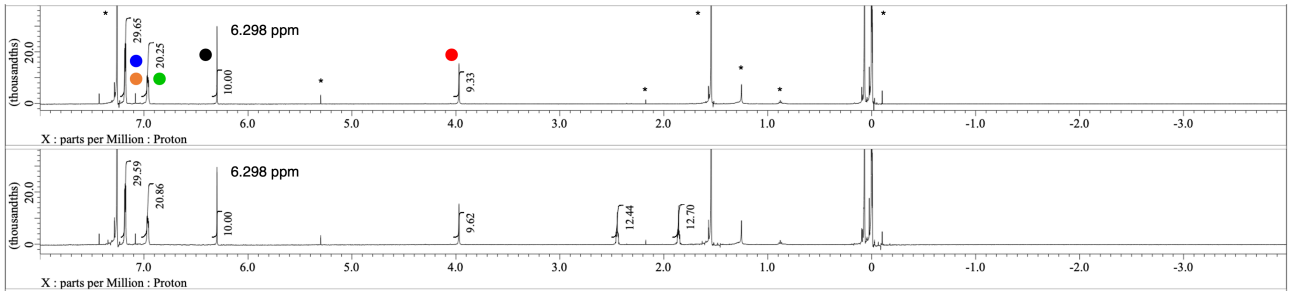

Figure S3-7. Comparison of ^{1}H (600 MHz) NMR spectra of **P5Ph** (0.5 mM) before (top) and after (bottom) addition of 1,4-dicyanobutane (6.3 equiv) in $CDCl_3$ at 25 °C. Peaks marked with * are due to residual solvents.

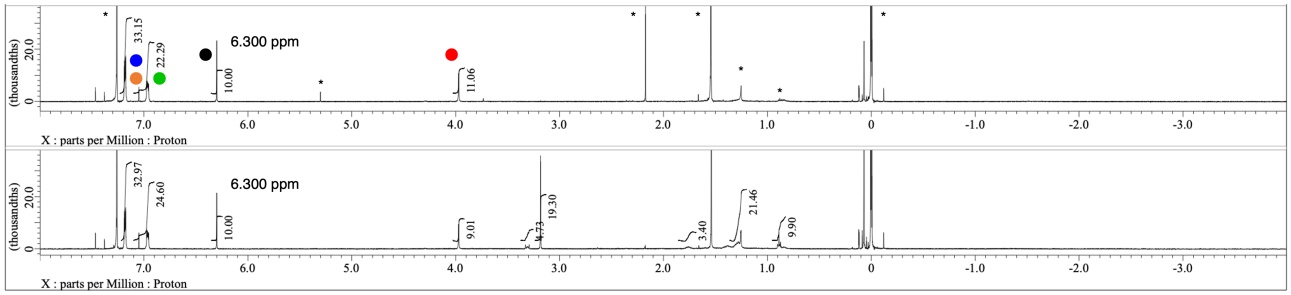

Figure S3-8. Comparison of ^{1}H (500 MHz) NMR spectra of **P5Ph** (0.1 mM) before (top) and after (bottom) addition of *n*-octyltrimethylammonium hexafluorophosphate (OTMA, 2.1 equiv) in $CDCl_3$ at 25 °C. Peaks marked with * are due to residual solvents.

4. High-resolution APCI-FT-MS

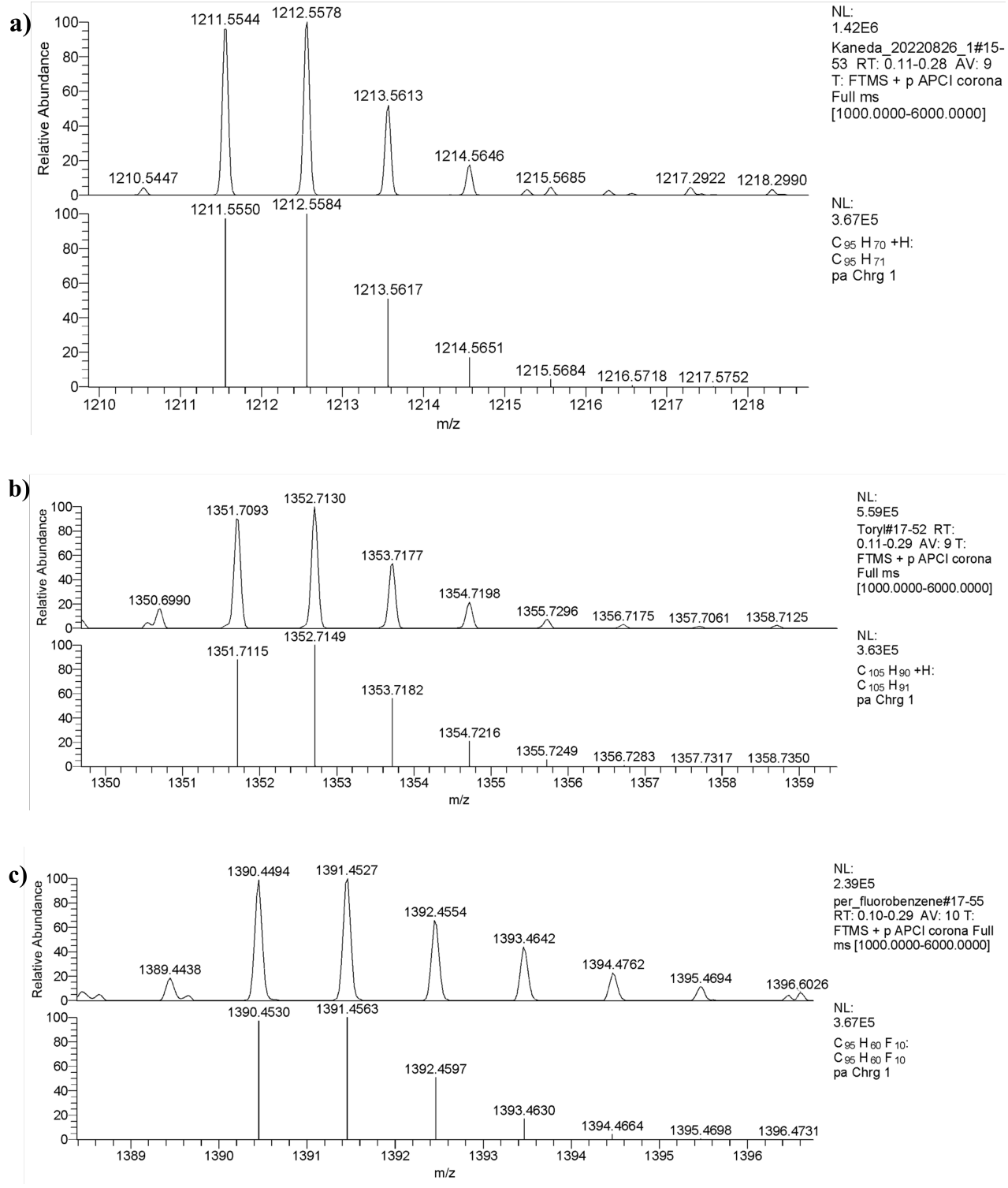

Figure S4-1. Observed (top) and simulated (bottom) high-resolution APCI-FT-MS of a) **P5Ph**, b) **P5PhMe**, and c) **P5PhF**.

5. X-Ray crystallographic analysis

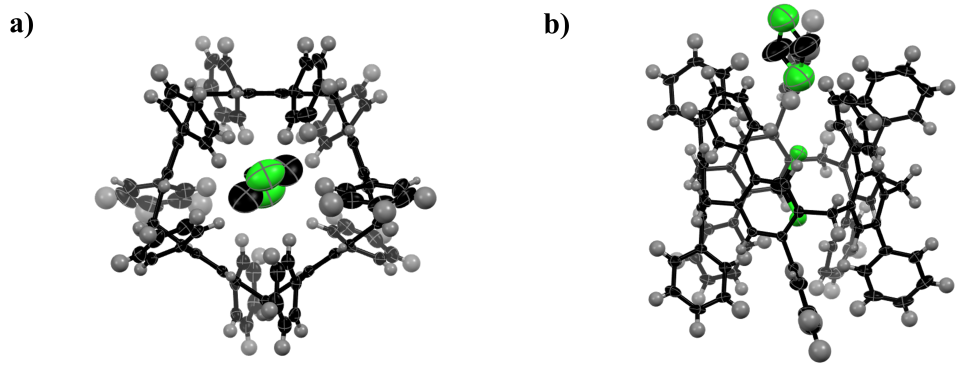

Figure S5-1. X-Ray crystal structure of **P5Ph**. a) Top view and b) side view. Thermal ellipsoids are scaled to 50% probability. The molecule was obtained as a half structure in the asymmetric unit and two dichloromethane molecules located at the special points were assigned without hydrogen atoms. Element colours: black, carbon; gray, hydrogen; light green, chlorine.

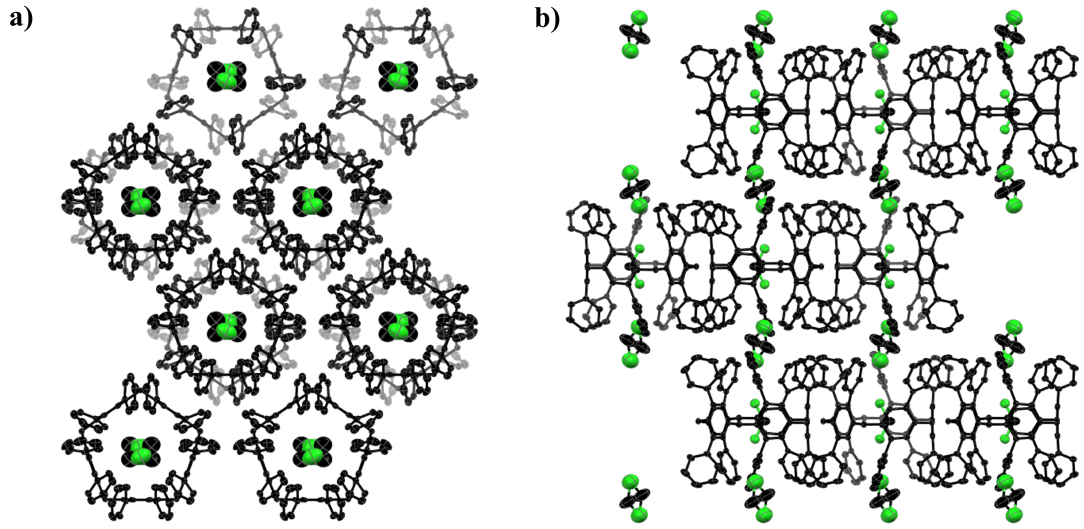

Figure S5-2. X-Ray packing structure of **P5Ph**. a) Top view and b) side view. Thermal ellipsoids are scaled to 50% probability. All hydrogen atoms are omitted for clarity. Element colours: black, carbon; light green, chlorine.

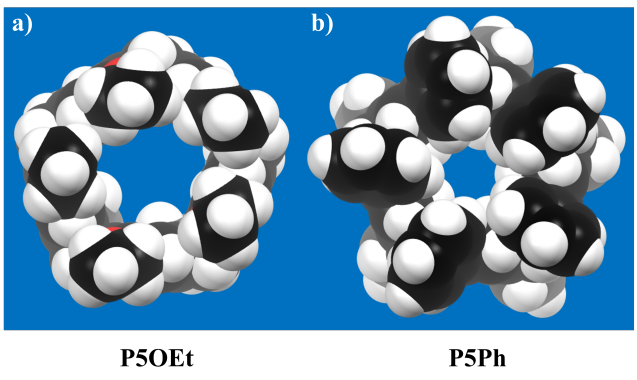

Figure S5-3. Space-filling representation of X-ray crystal structures of a) **P5OEt**[S7a] and b) **P5Ph**.

Table S5-1. Crystal data and structure refinements for **P5Ph**.

compound	**P5Ph**
formula	$C_{95}H_{70}$
	$2CH_2Cl_2$
solvent	CH_2Cl_2/*n*-hexane
MW	1210
T / K	143
crystal system	orthorhombic
space group	*Pbcn* (No. 60)
a / Å	14.015(3)
b / Å	20.406(4)
c / Å	25.223(6)
α / °	90
β / °	90
γ / °	90
V / Å^3	7214(3)
Z	8
ρ_{calc} / g cm^{-3}	1.211
completeness	0.997
R_1 [$I > 2\sigma(I)$]	0.0870
wR_2 (all data)	0.1863
GOF [$I > 2\sigma(I)$]	1.191
N (reflections)	5906/6336
N (parameters)	601
CCDC No.	2332554

The crystallographic data can be obtained free of charge from the Cambridge Crystallographic Data Centre (CCDC) via www.ccdc.cam.ac.uk/data_request/cif.

Table S5-2. Tilt angles of π-units relative to macrocycle backbones.[a]

compound	tilt angle [°]					
	unit 1	unit 2	unit 3	unit 4	unit 5	average
P5OEt·*n*-hexane[S7a]	1.72	1.01	1.55	2.90	2.79	1.99
P5OEt[S7b]	11.94	10.27	17.02	52.03	6.66	19.58
P5BFa[S7c]	48.59	23.39	51.32	12.06	11.40	29.35
P5F[S7c]	10.66	9.64	46.64	24.24	56.87	29.61
P5Ph·CH_2Cl_2	4.41	2.62	2.62	4.41	1.54	3.12

[a] tilt angle is measured from the average of the four dihedral angles that can be defined between benzene rings and methylene carbons on both sides of the benzene rings.

Table S5-3. Dihedral angles between aryl substituents and core benzene rings.[a]

compound	dihedral angle [°]					
	unit 1	unit 2	unit 3	unit 4	unit 5	average
P5BFa[S7c]	38.93	21.96	2.86	21.97	44.79	35.25
	70.00	27.05	57.50	40.62	26.86	
P5F[S7c]	14.46	50.83	39.76	32.38	36.30	38.24
	47.75	18.72	47.02	52.88	42.73	
P5Ph·CH_2Cl_2	59.41	61.32	63.67	74.34	71.84	66.12
	61.32	59.41	71.84	74.34	63.67	

[a] dihedral angle is defined between mean plane of 6 benzene carbons and that of aryl-substituent atoms.

6. UV/vis absorption and fluorescence spectra

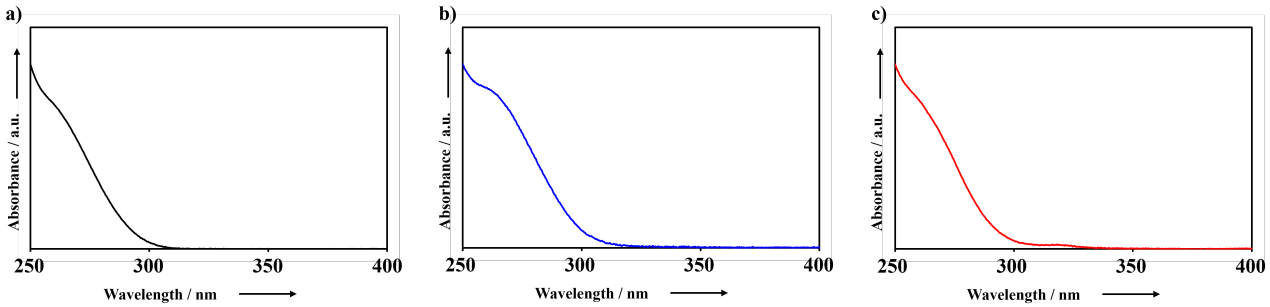

Figure S6-1. UV/vis absorption spectra of a) **P5Ph**, b) **P5PhMe**, and c) **P5PhF** in $CHCl_3$.

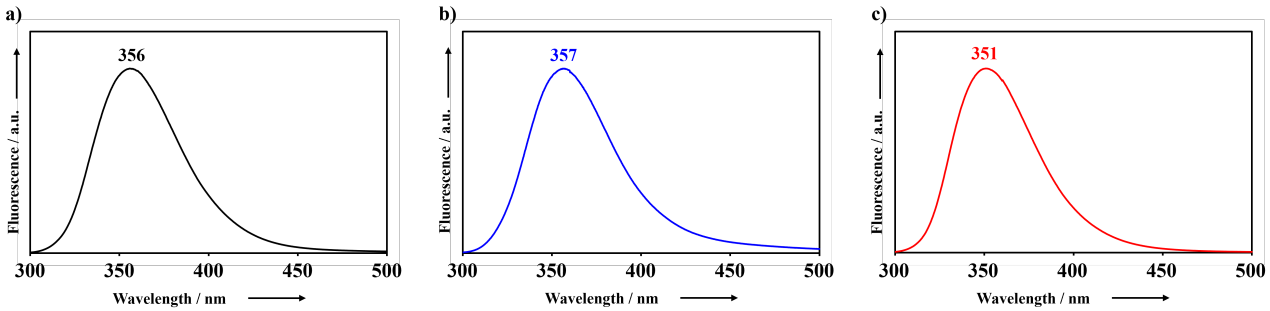

Figure S6-2. Fluorescence spectra of a) **P5Ph**, b) **P5PhMe**, and c) **P5PhF** in $CHCl_3$. Excitation wavelength was set at 255 nm for **P5Ph** and 260 nm for **P5PhMe** and **P5PhF**.

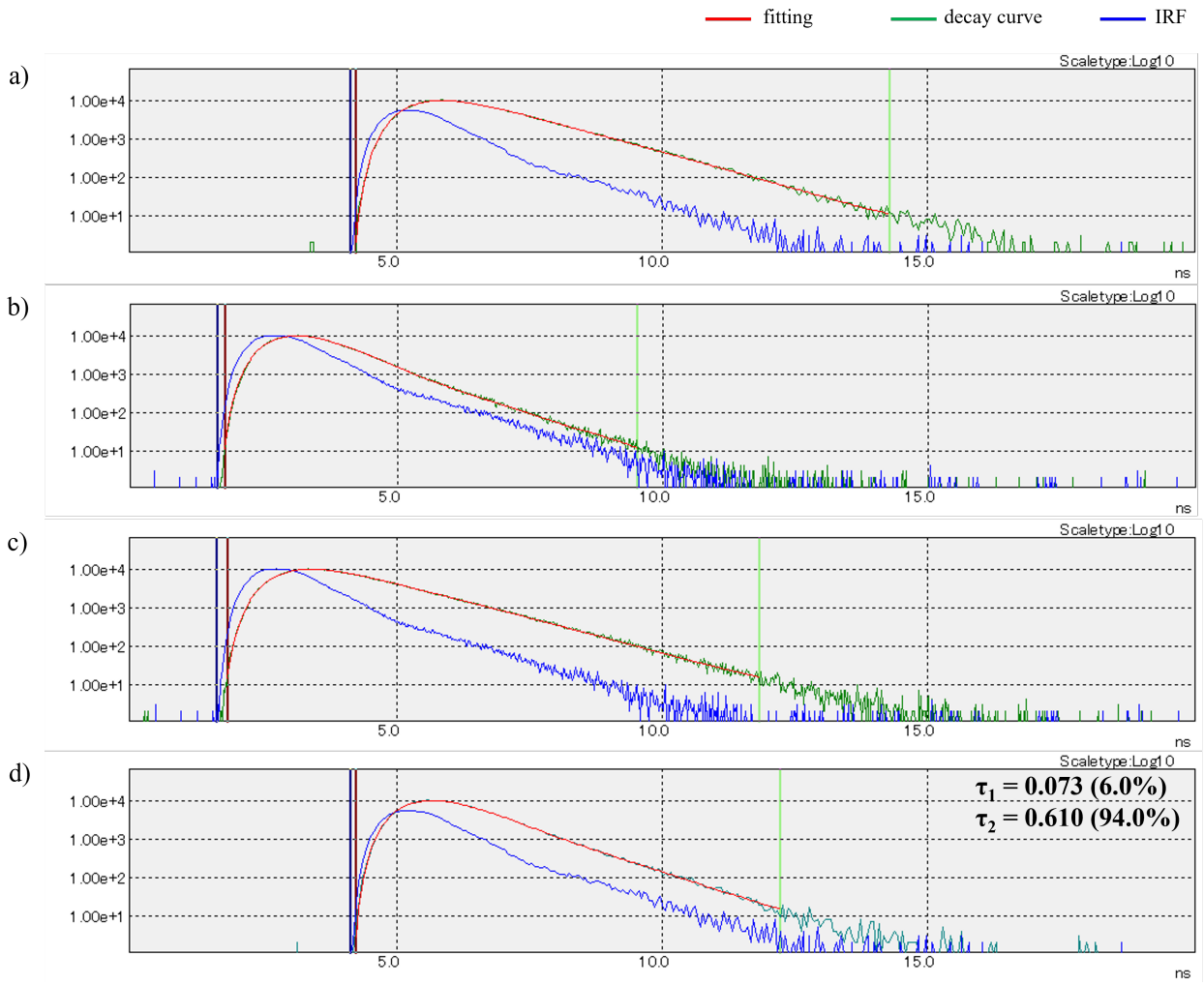

Figure S6-3. Fluorescence lifetime measurement of a) **P5Ph**, b) **P5PhMe**, c) **P5PhF**, and d) ***p*-terphenyl** in $CHCl_3$. Excitation wavelength was set at 280 nm. Detection wavelength was set at 355 nm for **P5Ph** and ***p*-terphenyl**, 357 nm for **P5PhMe**, and 255 nm for **P5PhF**.

Table S6-1. Summary of fluorescence properties.

	λ_{lum} [nm]	Φ_{lum}	τ [ns]	k_r [10^9 s^{-1}]	k_{nr} [10^9 s^{-1}]
P5Ph	355	0.18	0.98	0.18	0.84
P5PhMe	357	0.17	0.49	0.35	1.69
P5PhF	350	0.10	1.05	0.095	0.86
***p*-terphenyl**	355	0.37	0.61	0.61	1.03

The short fluorescence lifetimes indicated that the red-shifted emission of **P5Ph**, **P5PhMe**, and **P5PhF** was not due to their excimers but ascribed just to the conjugation within the *p*-terphenyl units and through-space interactions between the units at the excited states.

7. HPLC charts and chiroptical measurement

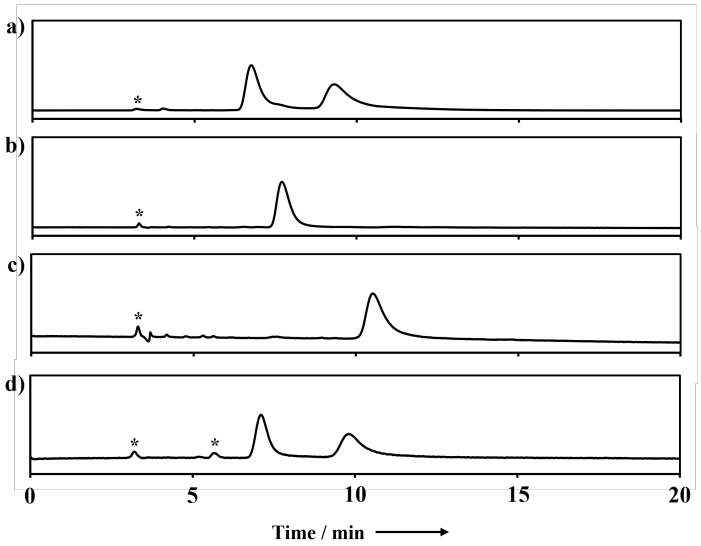

Figure S7-1. HPLC charts of a) racemate, b) 1st fraction, c) 2nd fraction, and d) 1st fraction after heating at 100°C for 12 h of **P5Ph** recorded as absorption of 250 nm light. Conditions: CHIRALPAK IA (ϕ = 4.6 mm, l = 250 mm) column; room temperature; flow rate = 1.0 mL/min; eluent = CH_2Cl_2/*n*-hexane (1/10). Peaks marked with * are due to injection and impurities.

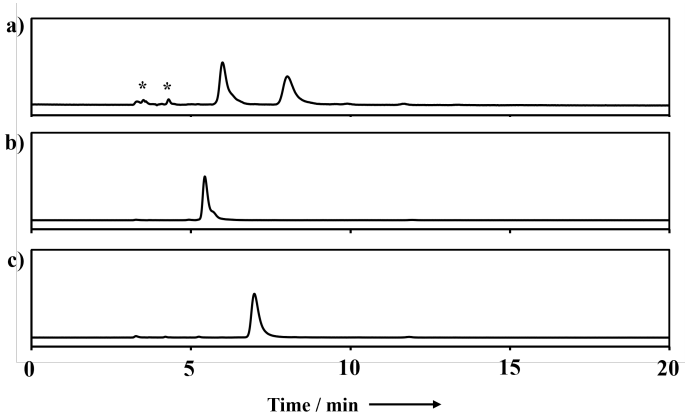

Figure S7-2. HPLC charts of a) racemate, b) 1st fraction, and c) 2nd fraction of **P5PhMe** recorded as absorption of 270 nm light. Conditions: CHIRALPAK IA (ϕ = 4.6 mm, l = 250 mm) column; room temperature; flow rate = 1.0 mL/min; eluent = CH_2Cl_2/*n*-hexane (1/10). Peaks marked with * are due to injection and impurities.

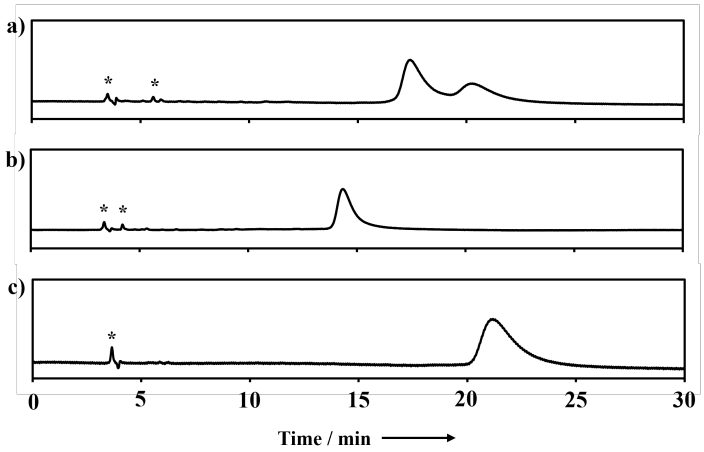

Figure S7-3. HPLC charts of a) crude sample, b) 1st fraction, and c) 2nd fraction of **P5PhF** recorded as absorption of 250 nm light. Conditions: CHIRALPAK IA (ϕ = 4.6 mm, l = 250 mm) column; room temperature; flow rate = 1.0 mL/min; eluent = CH_2Cl_2/*n*-hexane (1/10). Peaks marked with * are due to injection.

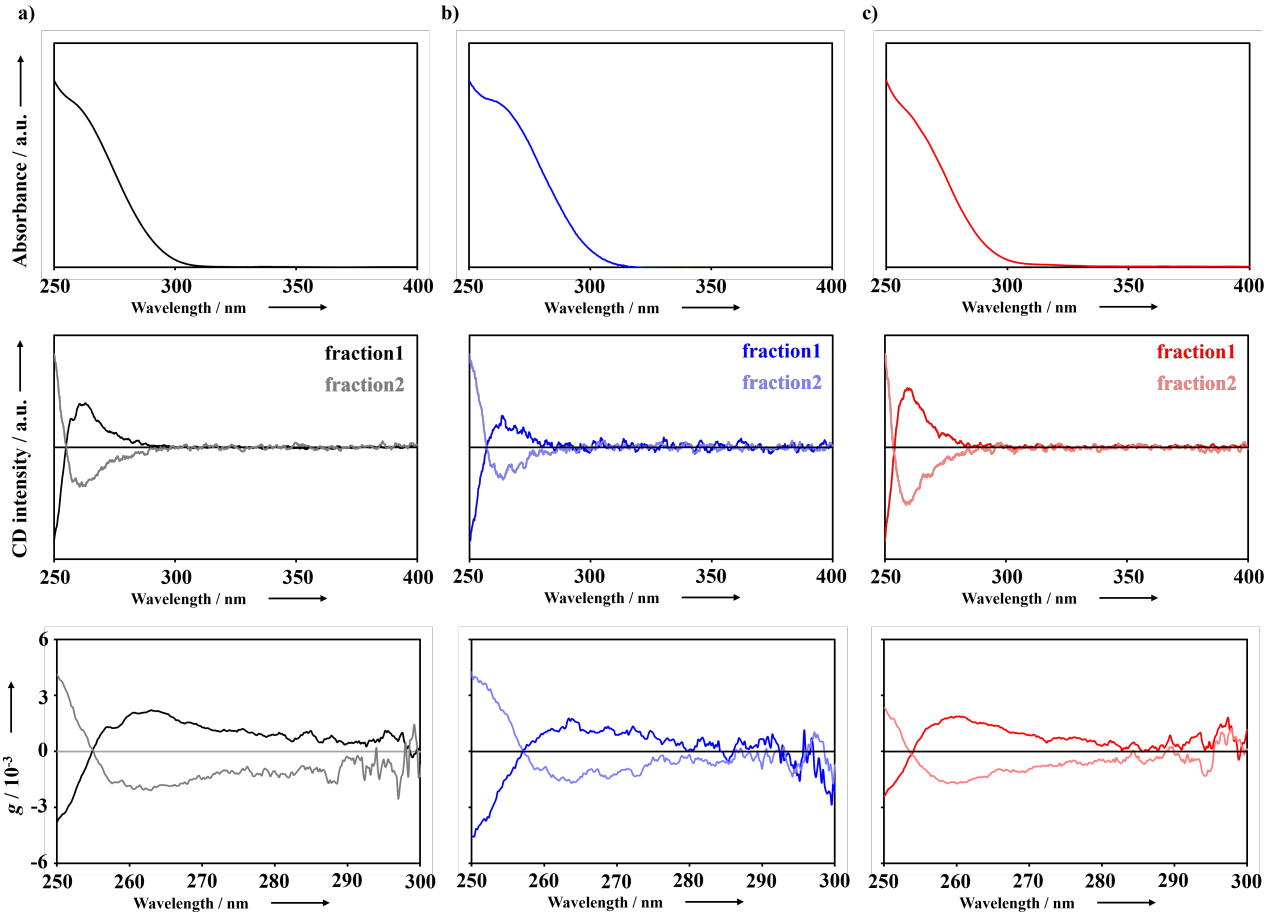

Figure S7-4. UV/vis absorption (top) and CD (middle) spectra in $CHCl_3$, and dissymmetry factor plots (bottom) of a) **P5Ph**, b) **P5PhMe**, and c) **P5PhF**.

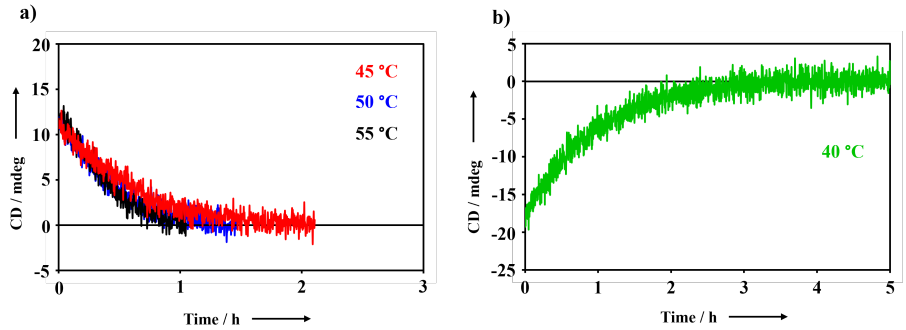

Figure S7-5. Decay profiles of CD intensities at 260 nm for solutions of a) 1st fraction of **P5Ph** at 45, 50, and 55 °C, and b) 2nd fraction of **P5Ph** at 40 °C in $CHCl_3$.

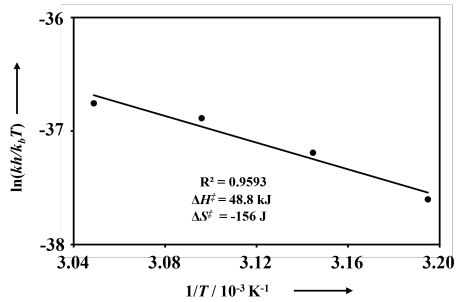

Figure S7-6. Eyring plot from the CD changes of **P5Ph**. Gibbs energy for activation ($\Delta G^{\ddagger}_{25\,°C}$) was determined to be 95.3 kJ mol^{-1}. The thermodynamic parameters, $\Delta H^{\ddagger}$ and $\Delta S^{\ddagger}$, were also determined from the slope and intercept by plotting $\ln(hk/k_BT)$ vs $1/T$.

$$ln\frac{hk}{k_BT} = -\frac{\Delta H^{\ddagger}}{R}\frac{1}{T} + \frac{\Delta S^{\ddagger}}{R}$$

where h, k_B, and R are the Planck constant, Boltzmann constant, and molar gas constant, respectively. k is the reaction rate constant. $\Delta G^{\ddagger}$ was obtained according to the following equation:

$$\Delta G^{\ddagger} = \Delta H^{\ddagger} - T\Delta S^{\ddagger}$$

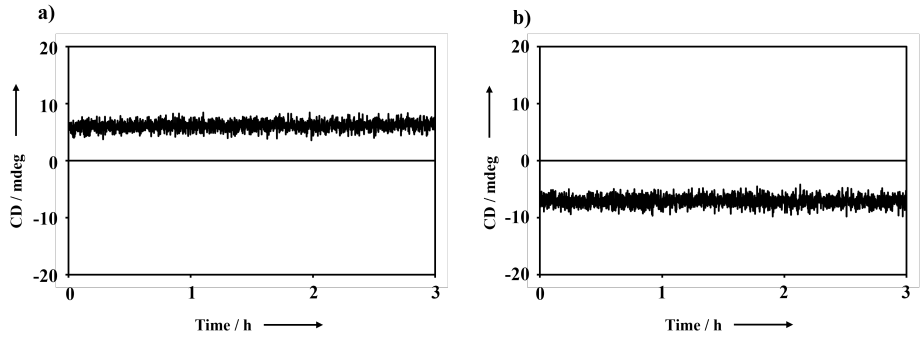

Figure S7-7. CD spectra at 80 °C of a) **P5PhMe** and b) **P5PhF** observed at 260 nm in 1,2-dichloroethane. 1,2-Dichloroethane is a much weaker guest for common pillar[5]arenes than 1,4-dicyanobutane. Therefore, small population of the guest-inclusion states led to no suppression of the racemization via unit rotation. The constant CD intensities were simply ascribed to intrinsically large Gibbs energies for activation ($\Delta G^{\ddagger}_{25\,^{\circ}C}$).

The high activation energies suggested that the C_2-symmetric isomers might be obtained after reaction because the C_2-isomers could be prevented from converting to the D_5-ones at reaction temperature. Recrystallization and purification by chiral HPLC might eliminate these isomers, but further investigation was difficult due to the low yields and presence of nine or less substituted pillar[5]arenes. Such intermediates could not be removed by column chromatography on silica gel and gel permeation chromatography. In addition, ^{1}H NMR spectra of the intermediates were hardly discerned from the C_2-symmetric isomers of the target products.

8. Theoretical calculations

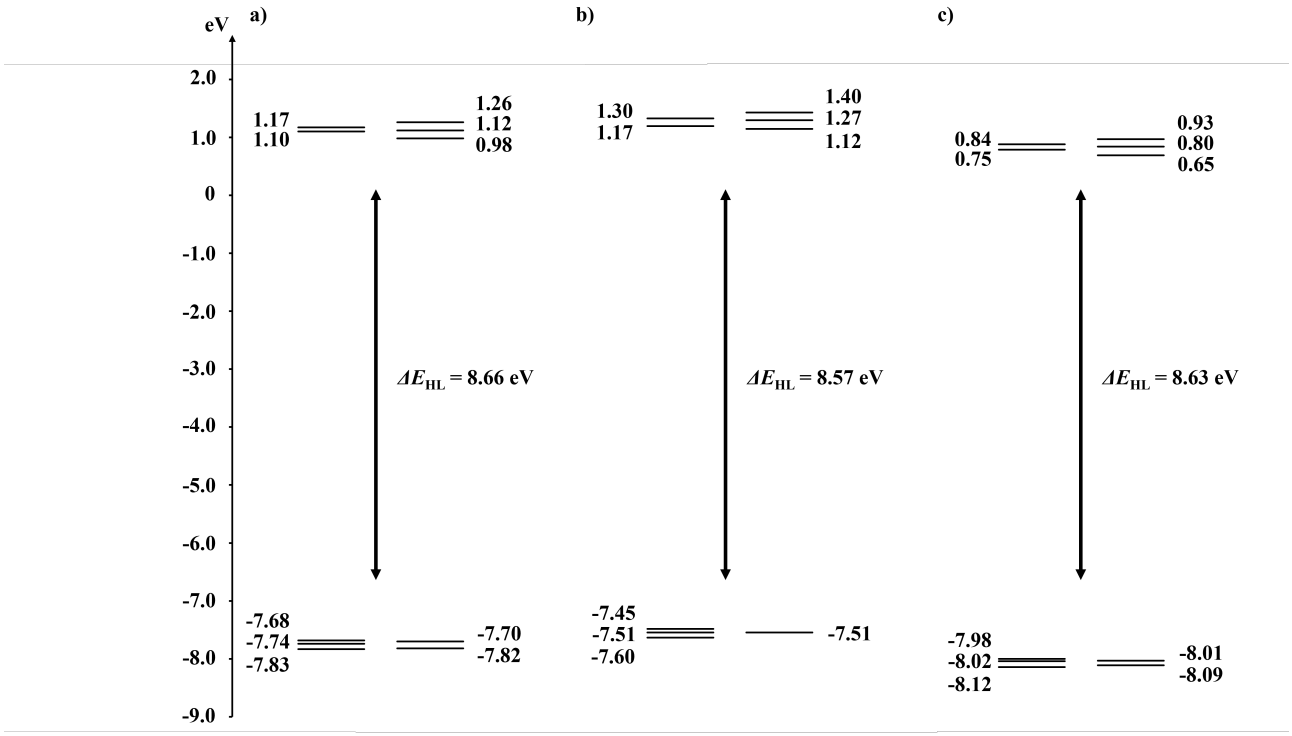

Figure S8-1. Energy diagrams of a) **P5Ph**, b) **P5PhMe**, and c) **P5PhF**.

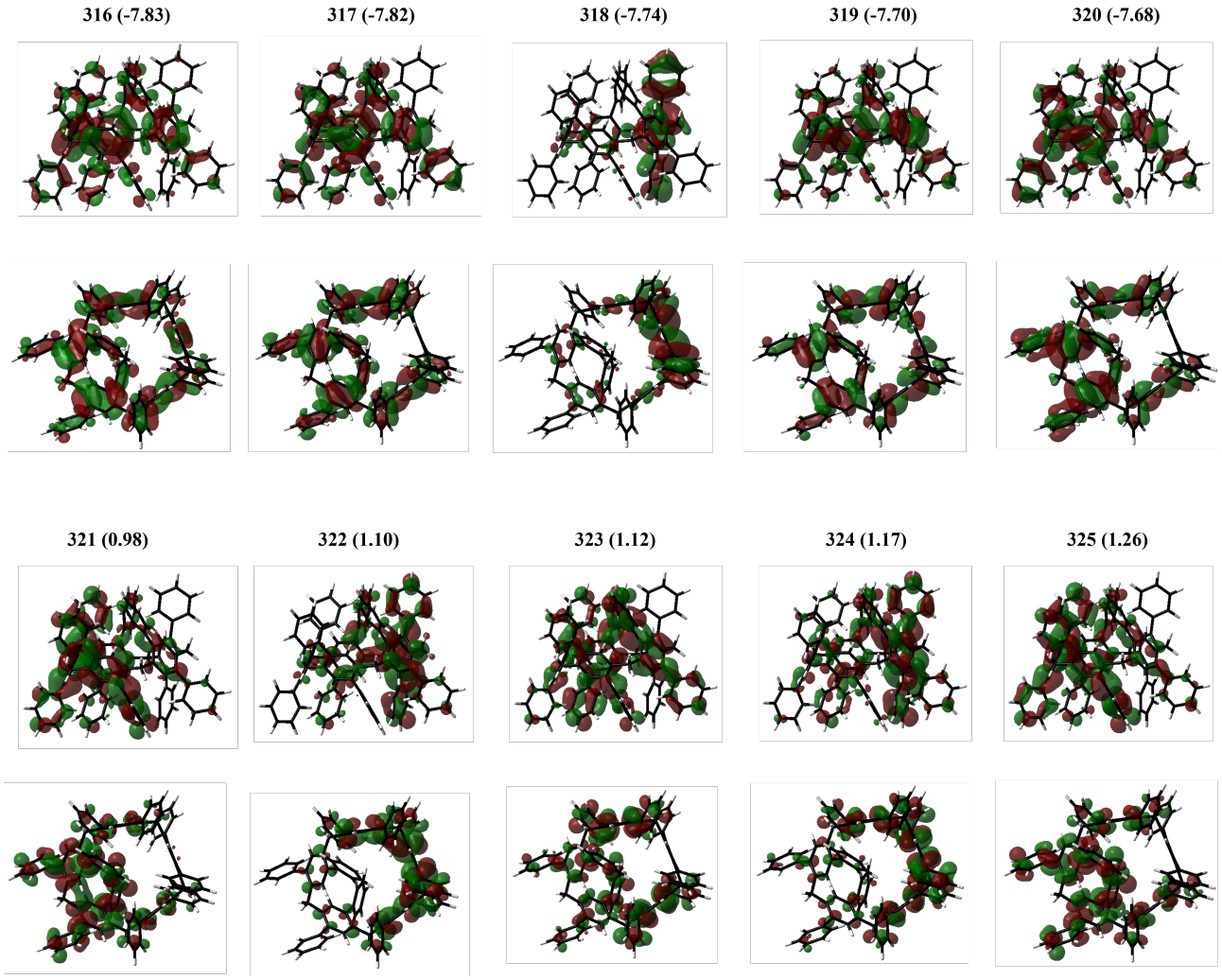

Figure S8-2. Kohn-Sham orbital representations of **P5Ph** (isovalue: 0.02).

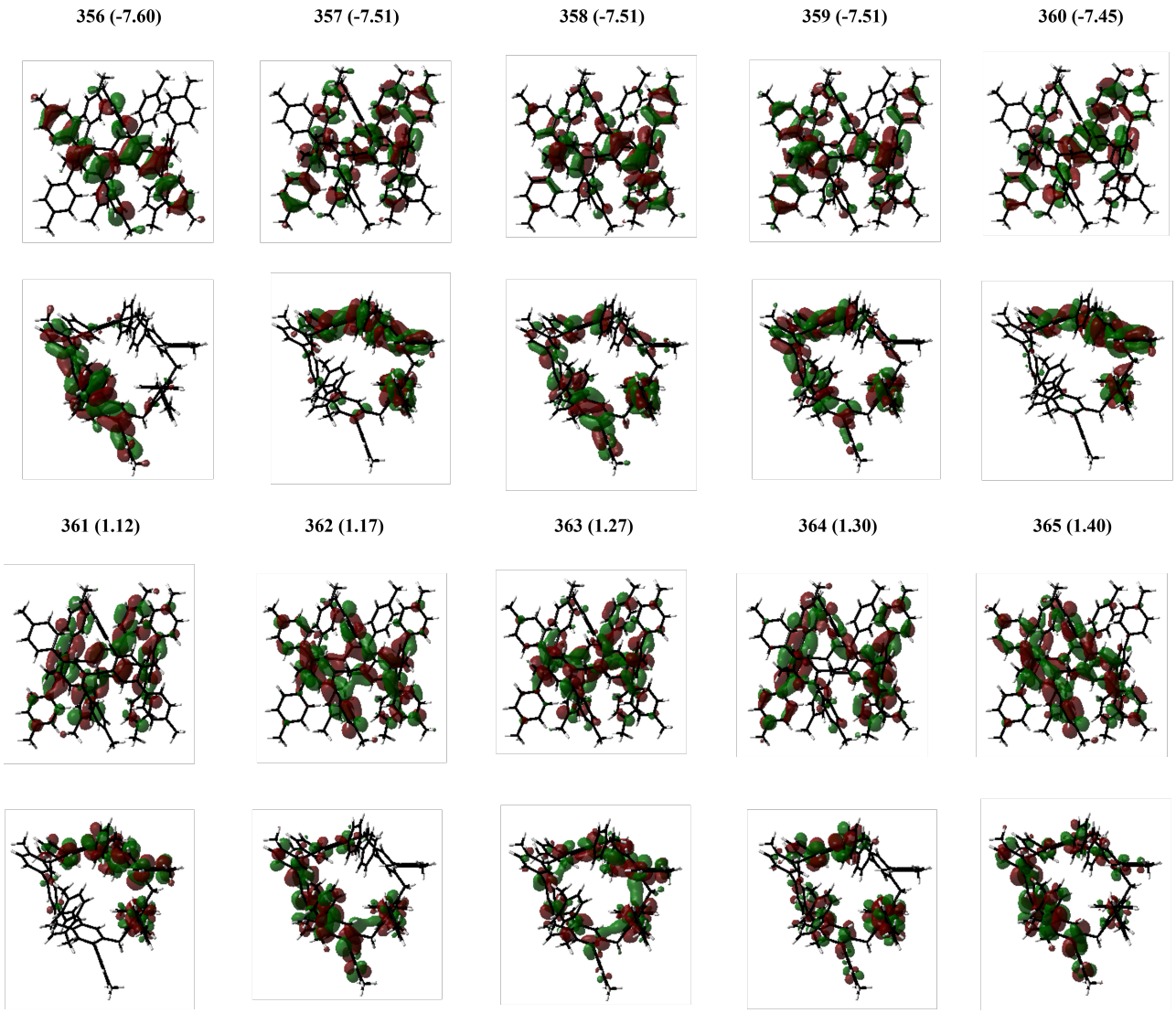

Figure S8-3. Kohn-Sham orbital representations of **P5PhMe** (isovalue: 0.02).

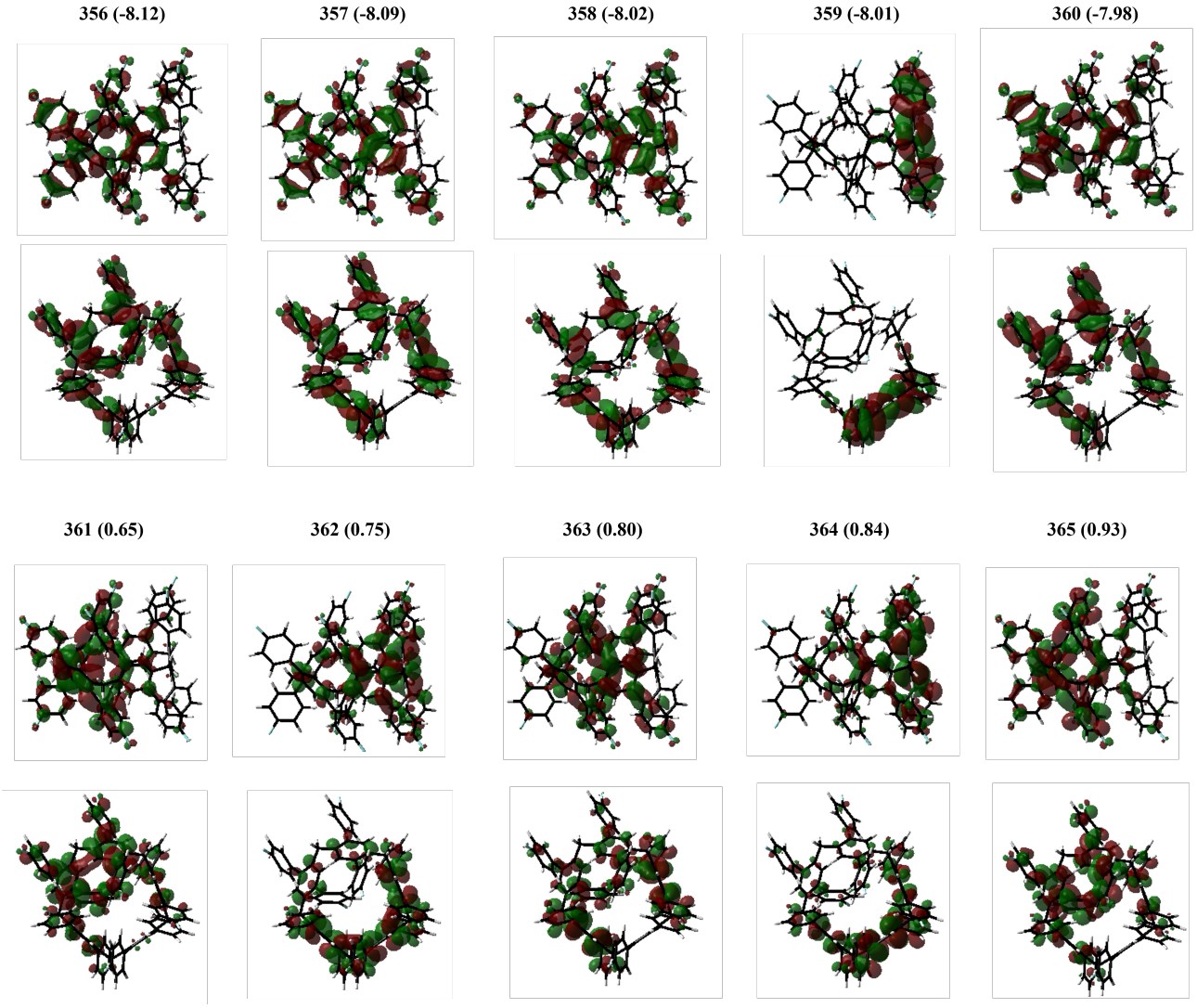

Figure S8-4. Kohn-Sham orbital representations of **P5PhF** (isovalue: 0.02).

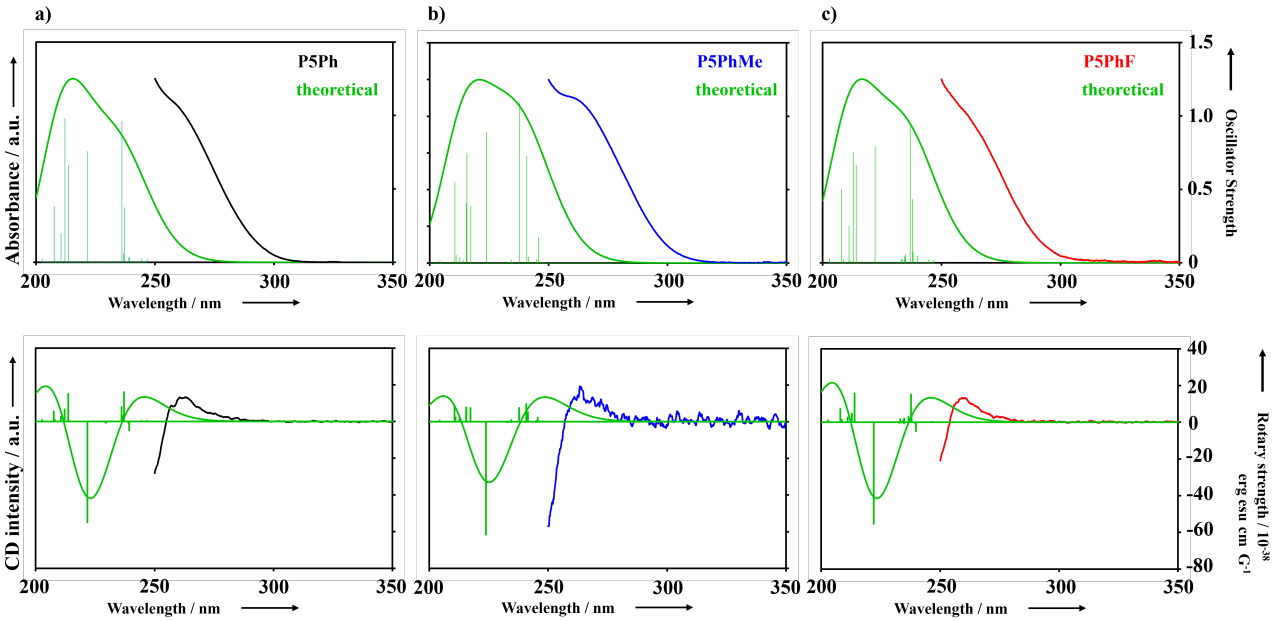

Figure S8-5. Comparison of experimental and theoretical spectra of a) **P5Ph**, b) **P5PhMe**, and c) **P5PhF**. UV/vis absorption (top) and CD (bottom) spectra. Calculated oscillator strengths and rotatory strengths are also shown with green vertical lines. Theoretical spectra are gained by setting half width at half height at 0.30 eV. From these results, each 1st fraction of **P5Ph**, **P5PhMe**, and **P5PhF** was assigned to R_P-enantiomer.

9. References

[S1] SHELXS-2013/1 and SHELXL-2018/3, programs for solution and refinement of crystal structures from diffraction data, G. M. Sheldrick, University of Göttingen, Göttingen (Germany): a) G. Sheldrick, T. Schneider, in *Methods in Enzymology*, Vol. 277, Elsevier, **1997**, pp. 319–343; b) G. M. Sheldrick, *Acta Cryst.* **2008**, *A64*, 112–122; c) G. M. Sheldrick, *Acta Cryst.* **2015**, *A71*, 3–8; d) G. M. Sheldrick, *Acta Cryst.* **2015**, *C71*, 3–8.

[S2] Yadokari-XG, Software for Crystal Structure Analyses, K. Wakita (2001); Release of Software (Yadokari-XG 2009) for Crystal Structure Analyses: C. Kabuto, S. Akine, T. Nemoto, E. Kwon, *J. Cryst. Soc. Jpn.* **2009**, *51*, 218–224.

[S3] Gaussian 16, Revision C.01, M. J. Frisch, G. W. Trucks, H. B. Schlegel, G. E. Scuseria, M. A. Robb, J. R. Cheeseman, G. Scalmani, V. Barone, G. A. Petersson, H. Nakatsuji, X. Li, M. Caricato, A. V. Marenich, J. Bloino, B. G. Janesko, R. Gomperts, B. Mennucci, H. P. Hratchian, J. V. Ortiz, A. F. Izmaylov, J. L. Sonnenberg, D. Williams-Young, F. Ding, F. Lipparini, F. Egidi, J. Goings, B. Peng, A. Petrone, T. Henderson, D. Ranasinghe, V. G. Zakrzewski, J. Gao, N. Rega, G. Zheng, W. Liang, M. Hada, M. Ehara, K. Toyota, R. Fukuda, J. Hasegawa, M. Ishida, T. Nakajima, Y. Honda, O. Kitao, H. Nakai, T. Vreven, K. Throssell, J. A. Montgomery, Jr., J. E. Peralta, F. Ogliaro, M. J. Bearpark, J. J. Heyd, E. N. Brothers, K. N. Kudin, V. N. Staroverov, T. A. Keith, R. Kobayashi, J. Normand, K. Raghavachari, A. P. Rendell, J. C. Burant, S. S. Iyengar, J. Tomasi, M. Cossi, J. M. Millam, M. Klene, C. Adamo, R. Cammi, J. W. Ochterski, R. L. Martin, K. Morokuma, O. Farkas, J. B. Foresman, D. J. Fox, Gaussian, Inc., Wallingford CT, **2019**.

[S4] B3LYP, Becke's three-parameter hybrid exchange functionals and the Lee–Yang–Parr correction functional: a) A. D. Becke, *J. Chem. Phys.* **1993**, *98*, 1372–1377; b) C. Lee, W. Yang, R. G. Parr, *Phys. Rev. B* **1988**, *37*, 785–789.

[S5] ϖB97X-D, long-range corrected (LC) hybrid density functional including empirical atom–atom dispersion corrections: J.-D. Chai, M. Head-Gordon, *Phys. Chem. Chem. Phys.* **2008**, *10*, 6615–6620.

[S6] T. Ogoshi, K. Umeda, T.-a. Yamagishi, Y. Nakamoto, *Chem. Commun.* **2009**, 4874–4876.

[S7] a) T. Ogoshi, R. Sueto, K. Yoshikoshi, Y. Sakata, S. Akine, T.-a. Yamagishi, *Angew. Chem. Int. Ed.* **2015**, *54*, 9849–9852; b) K. Jie, M. Liu, Y. Zhou, M. A. Little, A. Pulido, S. Y. Chong, A. Stephenson, A. R. Hughes, F. Sakakibara, T. Ogoshi, F. d. r. Blanc, G. M. Day, F. Huang, A. I. Cooper, *J. Am. Chem. Soc.* **2018**, *140*, 6921–6930; c) K. Kato, T. Kaneda, S. Ohtani, T. Ogoshi, *J. Am. Chem. Soc.* **2023**, *145*, 6905–6913.

[S8] a) L. Liu, Y. Zhang, Y. Wang, *J. Org. Chem.* **2005**, *70*, 6122–6125; b) L. Liu, Y. Zhang, B. Xin, *J. Org. Chem.* **2006**, *71*, 3994–3997.

10. Additional information

Comment S10-1: scale-up reactions

The reactions for **P5Ph**, **P5PhMe**, and **P5PhF** had been conducted using 40 mg of **P5OTf**, to obtain sufficient amounts of products for the full characterization. The crude mixtures were somewhat complicated, and the isolated yields were almost the same or lower than those starting with 20 mg of **P5OTf**. Although the complicated crude mixtures hampered clear discussion, we suppose that larger amounts of side products were produced because of the catalyst with a prolonged lifetime in scale-up systems and the lower yields were ascribed to the relatively low solubility of products in *n*-hexane-rich column eluents as compared with that of less symmetric side products.

Comment S10-2: changes in the amount of Pd catalyst

As suggested by entry 6 of Table 1, increase of the Pd catalyst would not improve the isolated yield. On the other hand, some crude mixtures in the optimum conditions included MS peaks of mono-triflate compounds by nine-fold substitution, which implied that large decrease of the Pd catalyst would be difficult. The catalyst loading of 100 mol% is 10 mol% for each reaction site, which can be regarded as a usual value for final steps of organic materials synthesis.

Comment S10-3: attempted ligand-free reaction and reactions with other organoboron reagents

To circumvent sterically bulky intermediates, a ligand-free reaction[S8] with phenylboronic acid and $Pd(OAc)_2$ was attempted. However, ^1H NMR spectrum of the crude mixture included **P5OTf** and $PhB(OH)_2$ but did not show any peak at 6.5–6.0 ppm (Figure S10-1b). MS result indicated the presence of **P5OTf** and absence of target **P5Ph** or nine-fold-substituted compound (Figure S10-2c). In addition, the optimum conditions with Pd-PEPPSI-iPr were tested using phenylboronic acid pinacol ester or potassium trifluoro(phenyl)borate instead of phenylboronic acid, but their crude mixtures did not indicate improvement of the reaction (Figure S10-1c,d and S10-2a,b).

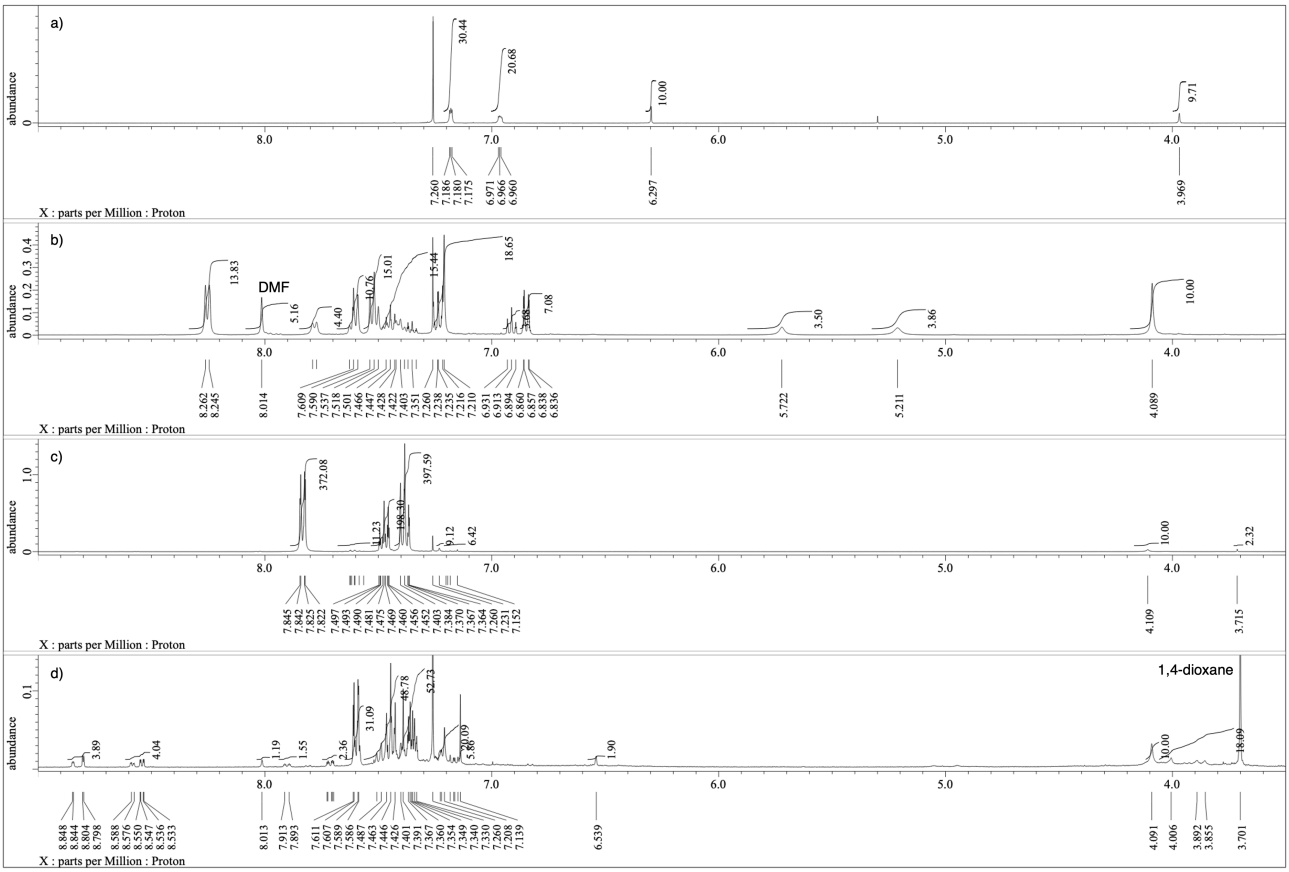

Figure S10-1. Comparison of a) ^{1}H (600 MHz) NMR spectrum of isolated **P5Ph** in $CDCl_3$ at 25 °C and b,c,d) ^{1}H (400 MHz) NMR spectra for the crude mixtures of **P5Ph** in $CDCl_3$ at 25 °C. Reagents and conditions: b) phenylboronic acid (30 equiv), $Pd(OAc)_2$ (100 mol%), Na_2CO_3 (20 equiv), DMF/H_2O (7/6), 100 °C, 24 h; c) phenylboronic acid pinacol ester (30 equiv), Pd-PEPPSI-iPr (100 mol%), K_2CO_3 (20 equiv), 1,4-dioxane, 100 °C, 24 h; d) potassium trifluoro(phenyl)borate (30 equiv), Pd-PEPPSI-iPr (100 mol%), K_2CO_3 (20 equiv), 1,4-dioxane, 100 °C, 24 h.

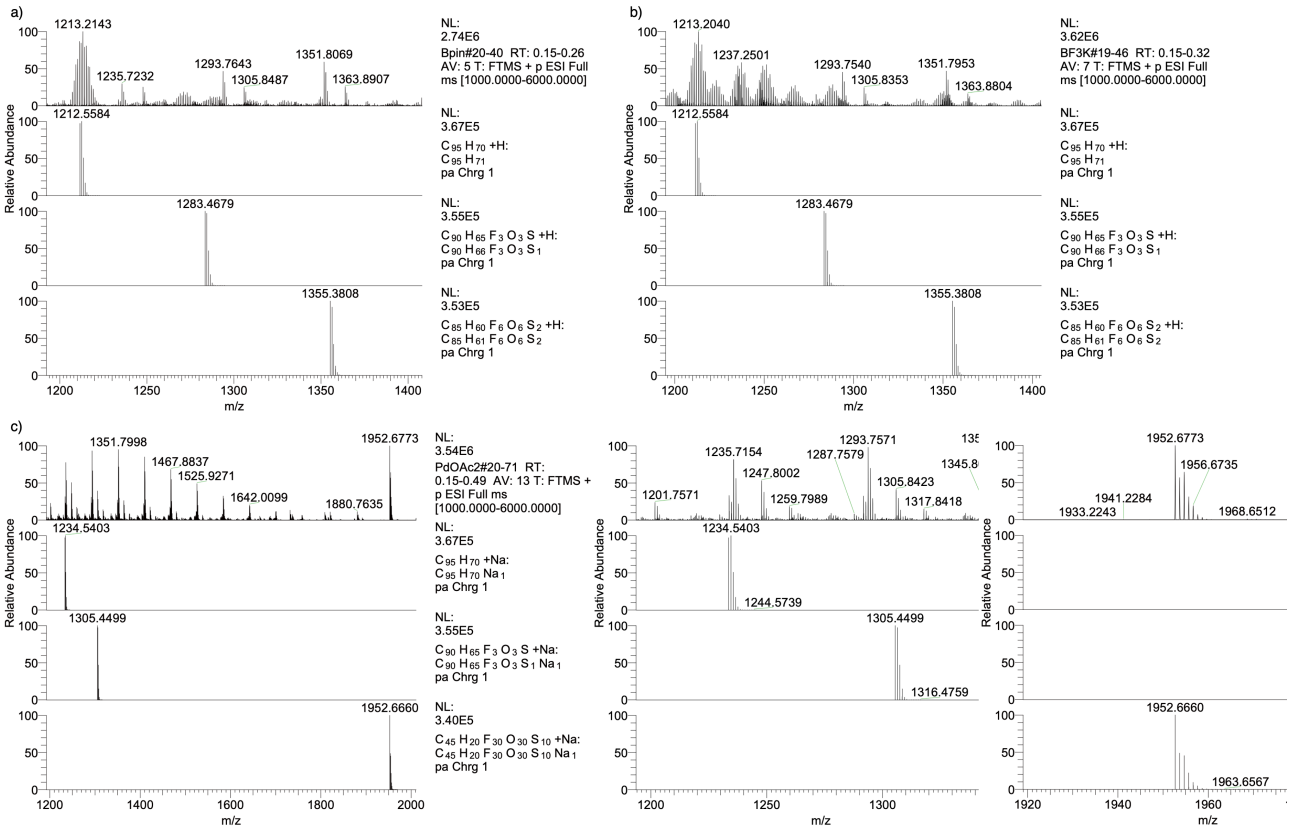

Figure S10-2. High-resolution ESI-FT-MS for the crude mixture of **P5Ph** after various reaction conditions. Reagents and conditions: a) phenylboronic acid pinacol ester (30 equiv), Pd-PEPPSI-iPr (100 mol%), K_2CO_3 (20 equiv), 1,4-dioxane, 100 °C, 24 h; b) potassium trifluoro(phenyl)borate (30 equiv), Pd-PEPPSI-iPr (100 mol%), K_2CO_3 (20 equiv), 1,4-dioxane, 100 °C, 24 h; c) phenylboronic acid (30 equiv), $Pd(OAc)_2$ (100 mol%), Na_2CO_3 (20 equiv), DMF/H_2O (7/6), 100 °C, 24 h.

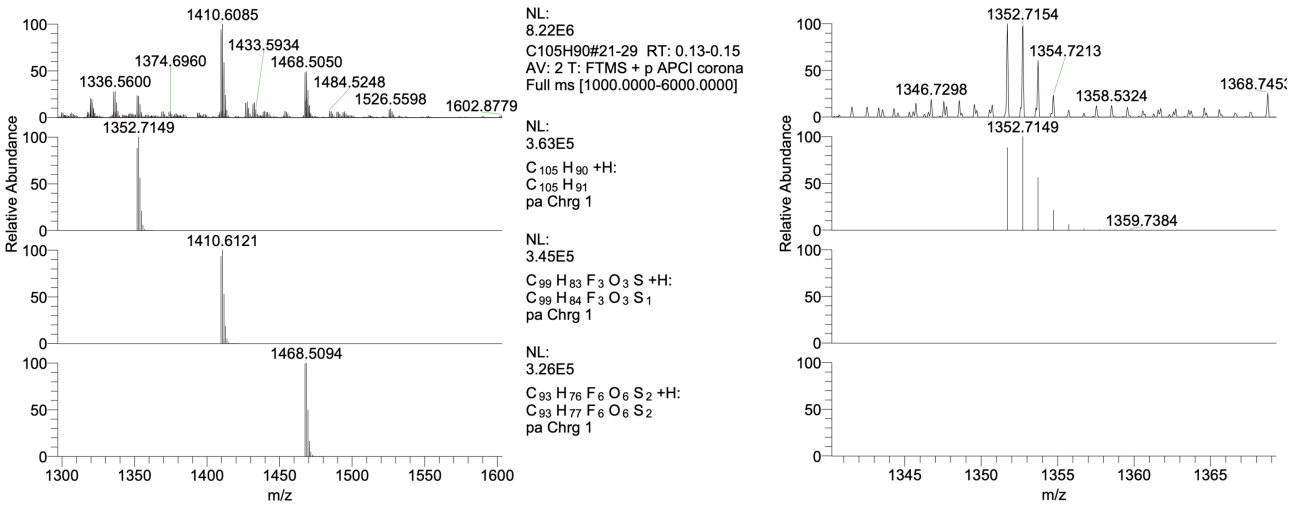

Figure S10-3. High-resolution ESI-FT-MS for the crude mixture of entry 3 in Table 1 (synthesis of **P5PhMe**, reagents and conditions: 4-methylphenylboronic acid (30 equiv), XPhos Pd G3 (100 mol%), K_2CO_3 (20 equiv), 1,4-dioxane/mesitylene/H_2O (4/4/1), 120 °C, 20 h). On the right, a MS region for **P5PhMe** is displayed.

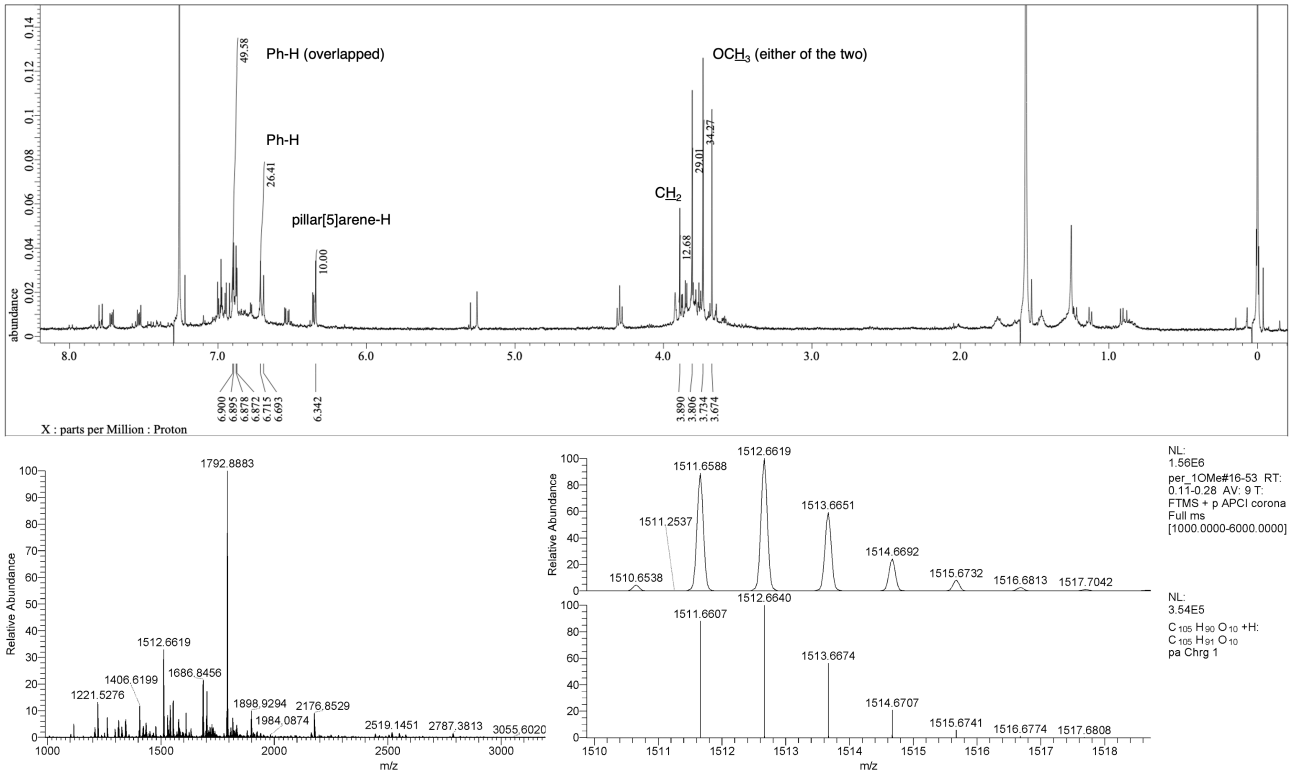

Figure S10-4. ^{1}H (400 MHz) NMR spectra in $CDCl_3$ at 25 °C (top) and high-resolution APCI-FT-MS (bottom) of a mixture containing **P5PhOMe**.

Comment S10-4: intermolecular interactions in the single crystal

Because the molecule was obtained as a half structure in the asymmetric unit and two dichloromethane molecules located at the special points were assigned without hydrogen atoms, we refrained from discussing CH/π and CH/Cl interactions with distance values in the main text. However, the location implies that the dichloromethane inside the macrocycle can have both interactions and the outside one can form multi-point CH/Cl interactions.

Comment S10-5: alert B for X-ray analysis

PLAT910_ALERT_3_B Missing # of FCF Reflection(s) Below Theta(Min). 12 Note

2 0 0, 1 1 0, 0 2 0, 1 1 1, 0 2 1, 1 2 1,

0 0 2, 1 0 2, 1 1 2, 0 2 2, 1 2 2, 1 1 3,

For some crystals, it is difficult to collect small-theta reflections using the single-crystal X-ray apparatus with Mo-Kα radiation.

PLAT964_ALERT_2_B SHELXL WEIGHT Par. Values in CIF & RES Differ .. Please Check

The IUCr instruction is as follows:

“PLAT964 Type_2 Test for consistency of SHELXL weight parameters in CIF & embedded RES

Two weight parameter values reported in the CIF weight expression string (_refine_ls_weighting_details) are found to differ from those archived in the WGHT parameter value list in the embedded RES file. The latter values are assumed to be the correct ones as part of the final refinement. Recreation of the FCF from the embedded .ins & .hkl will result in inconsistent wR2 and S values and associated ALERTS in the checkCIF report when those weight parameter values differ. Please also check the proper format of the SHELXL weight expression string.”

The wR2 and S values are consistent in CIF and embedded RES. Related information in the CIF is as follows:

_refine_ls_weighting_details

'w=1/[¥s^2^(Fo^2^)+(0.0516P)^2^+10.5000P] where P=(Fo^2^+2Fc^2^)/3'

_refine_ls_number_reflns 6336

_refine_ls_number_parameters 601

_refine_ls_number_restraints 648

_refine_ls_R_factor_all 0.0930

_refine_ls_R_factor_gt 0.0870

_refine_ls_wR_factor_ref 0.1863

_refine_ls_wR_factor_gt 0.1826

_refine_ls_goodness_of_fit_ref 1.191

_refine_ls_restrained_S_all 1.135

_refine_ls_shift/su_max 0.001

_refine_ls_shift/su_mean 0.000

WGHT 0.054500 10.500000

REM

REM wR2 = 0.1863, GooF = S = 1.191, Restrained GooF = 1.135 for all data

REM R1 = 0.0870 for 5906 Fo > 4sig(Fo) and 0.0930 for all 6336 data

REM 601 parameters refined using 648 restraints

END

WGHT 0.0550 9.7915

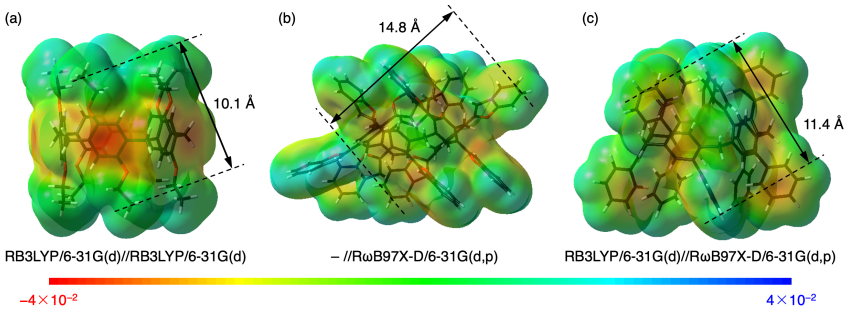

Figure S10-5. Electrostatic potential maps of a) **P5OEt**, b) **P5BFa**, and c) **P5Ph** (isovalue: 0.0004). Side views are displayed because the crushed structure of **P5BFa** and high bulkiness around top and bottom of the cavity of **P5Ph** hamper clear view of the insides of cavities.

In addition to the crushed cavities, **P5BF** has several isomers and high conformational flexibility, which can affect host–guest ability in solution. For the structures in this figure, the cavity sizes cannot be defined consistently. Therefore, atomic distance is indicated for the carbon atoms on both sides in each unit.